Far-infrared sphere resonance in isolated superconducting particles

T. W. Noh, S. G. Kaplan, and A. J. Sievers
Laboratory of Atomic and Solid State Physics and Materials Science Center, Cornell University, Ithaca, New York 14853

(Received 27 April 1989; revised manuscript received 4 August 1989)

A strong electric-dipole resonance has been observed in the far-infrared response of small isolated superconducting particles of $La_{2-x}Sr_xCuO_{4-y}$, $Nd_{1.85}Ce_{0.15}CuO_4$, and $Bi_4Ca_3Sr_3Cu_4O_z$, but not in $YBa_2Cu_3O_{7-y}$. Because of the small-particle boundary conditions, the bulk conductivity δ function of the superconducting condensate translates from zero to finite frequency, so that sphere resonance studies of the oxide superconductors provide important information about a dc property, the London penetration depth. The far-infrared data show that the frequency and strength of this resonance decrease as the temperature approaches T_c from below, and no resonance is observed above T_c. The effect of a magnetic field on this feature is similar to that produced by raising the temperature. The $La_{2-x}Sr_xCuO_{4-y}$ system has been studied in some detail. By increasing the Sr doping it has been possible to drive the resonance frequency above the gap. An analysis based on the Maxwell-Garnett formalism is used to explain the observed changes in the resonant features. This analysis shows that for $La_{2-x}Sr_xCuO_{4-y}$ the superconducting sphere resonance is polarized along the c axis of the particles. Moreover, the observed behavior of the resonant feature fixes some inequalities that the normal and superconducting carrier parameters must satisfy, namely, that the c-axis energy-gap frequency is larger than the sphere resonance frequency but both of these frequencies are smaller than the normal-state carrier scattering rate. Since the sphere resonance position and the London penetration depth $\lambda(T)$ are closely related to the oscillator strength of the superconducting condensate, we can show that $\lambda(0)=5.8$ μm along the c axis for $x=0.15$. The temperature dependence of $\lambda(T)$ for this sample follows the prediction of the empirical "two-fluid" approximation, but the behavior of samples for other values of x cannot be explained by any limiting case of BCS theory. Possible mechanisms for the large background absorption and the resonance line broadening are also discussed. This absorption below the gap may stem from disorder-induced lattice absorption, an unavoidable consequence of nonstoichiometric materials.

I. INTRODUCTION

Historically, far-infrared (fir) spectroscopy was essential in demonstrating the existence of the superconducting energy gap,[1] but the technique was quickly replaced by the more sensitive electron tunneling spectroscopy.[2] So far this increased sensitivity has not been of much use in analyzing the high-T_c superconductors[3] because of the nature of the superconductivity and the sample surface quality. These materials are strongly Type II, and the coherence length is very small,[4] ~ 10 Å. Since tunneling experiments probe only a coherence length into the sample surface, excellent surface quality is essential to measure bulk properties. To date these transition-metal oxides have notoriously poor surfaces, and tunneling results have been inconsistent and highly junction dependent. On the other hand, the fir spectroscopic technique probes a skin depth, of order 1 μm, so the surface quality condition can be relaxed somewhat.

Because of this realization, much work has been done to characterize the far-infrared reflectivity of these materials, in both polycrystalline[5-7] and single-crystal form.[8-14] However, since the materials are so complex and unusual, unique electrodynamic parameters are yet to be extracted from these measurements. For example, these new superconductors are highly anisotropic,[15] with metallic hole (or electron) conduction occurring in the Cu-O planes and carrier hopping or tunneling between these planes giving rise to a much smaller conductivity in the c direction, perpendicular to the Cu-O planes. For sintered pellets, composed of randomly oriented highly anisotropic grains, the interpretation of the reflectivity data must be approached with care in order to determine the dielectric function of the grains themselves.[6] Even in this case it has not yet been possible to find a superconducting gap value which is consistent either with BCS (Ref. 16) or with the single crystal[10-12] or with thin-film[17] results.

It is perhaps surprising that single crystals have not yet resolved this problem but high quality single crystals are not only difficult to grow but also to stabilize and maintain.[18] One controversy in the interpretation of the available single-crystal data is the peak observed in the ratio of the far-infrared reflectivity of the superconducting and normal states. It is interpreted as the signature of the energy gap 2Δ by some workers,[10-12] but the same structure is interpreted to be simply related to a zero crossing of the real part of the dielectric response by others.[7,14]

Even the normal-state reflectivity is subject to varying interpretation. The temperature-dependent reflectivity has been explained both by a two-band model consisting of a temperature-dependent Drude term and

temperature-independent interband transition,[12,14] and by a model with a frequency- and temperature-dependent scattering rate.[6,12,13]

Compared to the extensive experimental work on polycrystalline[5-7] and single-crystal[8-14] samples, little effort has gone into examining the electrodynamics of the isolated particle form of high-T_c superconductors[19,20] even though in the past in many materials,[21,22] especially free-electron-like metals, the single-particle form has been used to probe the dielectric function of the bulk. The idea behind such an approach is to investigate isolated grains of size much smaller than the wavelength of the radiation so that the electrostatic approximation applies. In this limit the electric dipole moment of the particle is[23]

$$\mathbf{p}=\frac{\epsilon(\omega)-\epsilon_h}{\epsilon(\omega)+2\epsilon_h}a^3\mathbf{E}\ , \tag{1}$$

where $\epsilon(\omega)$ is the dielectric function of the bulk metal, ϵ_h the dielectric constant of the transparent host containing the particle of diameter a, and $\mathbf{E}$ is the electric field. A strong electric dipole resonance occurs when the denominator in Eq. (1) becomes very small which occurs when

$$\mathrm{Re}[\epsilon(\omega_{sr})+2\epsilon_h]\approx 0$$

and (2)

$$\mathrm{Im}[\epsilon(\omega_{sr})+2\epsilon_h]\ll 1\ .$$

In other words, if the particle is not too lossy, a strong resonant absorption will occur at a frequency where the dielectric constant of the bulk is close to $-2\epsilon_h$. This absorption feature is called a "sphere resonance" since it is not an intrinsic property of the bulk material but comes from the boundary conditions of the spherical particle.[21]

The relationship between the bulk dielectric function and the small particle response is well known for a simple Drude metal, whose dielectric constant can be written as

$$\epsilon(\omega)=1-\omega_p^2/(\omega^2+i\omega/\tau)\ ,$$

where ω_p and τ^{-1} are the plasma frequency and the scattering rate of the metal, respectively. As shown in Fig. 1(a), the real part of the conductivity of the bulk material $\sigma_1(\omega)$ is a Lorentzian centered at zero frequency, and the real part of the dielectric function, $\epsilon_1(\omega)$, crosses zero near ω_p as long as $\omega_p\gg\tau^{-1}$. The response for a small particle is a Lorentz oscillator centered at the sphere resonance frequency,

$$\omega_{sr}\approx\omega_p/(1+2\epsilon_h)^{1/2}\ .$$

As indicated in Fig. 1(b), the linewidth of the Lorentz oscillator is the same as τ^{-1} if the particle size is larger than the electron mean free path. Moreover, since the sum rule[24] $\int\sigma_1(\omega)d\omega=\omega_p^2/8$ is the same whether the metal is in the bulk or single-particle form independent of the scattering time, measurement of the line strength provides another method to measure the plasma frequency. On the other hand, if the carrier scattering frequency is small ($\omega_p\tau\sim 1$), then the resonance will not occur because the imaginary part of the dielectric function,

$$\epsilon_2(\omega_{sr})>|\epsilon_1(\omega_{sr})-1|\ .$$

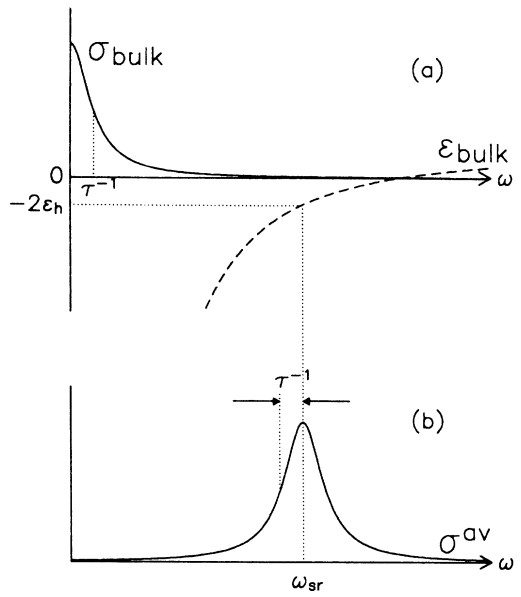

FIG. 1. Electrodynamic response functions for the bulk and small particle forms of a typical metal: (a) Conductivity and dielectric constant of a bulk metal, and (b) the effective conductivity for a small particle of the same material, showing the resonance where $\epsilon_{bulk}\approx-2\epsilon_h$. Note that the width of the conductivity curve in each case is given by the bulk carrier scattering rate.

What is the analogous situation for superconductors in the small particle form? We show the expected results for the sphere resonance in the five cases listed in Table I. For the limit where $\omega_p\tau\gg 1$ in the normal state there are two simple cases which can be considered either (I) $2\Delta\tau\gg 1$ or (II) $2\Delta\tau\ll 1$ where 2Δ is the superconducting energy gap. In Case I, the entire normal-state conductivity spectrum collapses into the δ function at zero temperature [Fig. 2(a)] so that the sphere resonance would

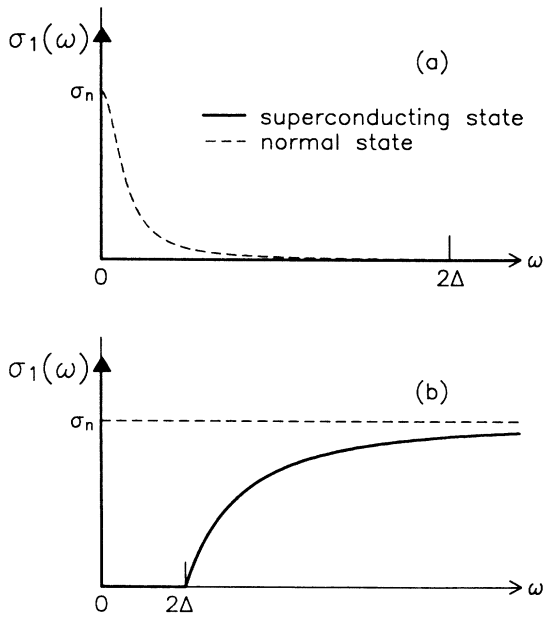

FIG. 2. Conductivity of a superconductor in two limiting cases: (a) $1/\tau\ll 2\Delta$ and (b) $1/\tau\gg 2\Delta$.

narrow dramatically upon cooling below the transition temperature. In Case II, as shown in Fig. 2(b), $\sigma_{1s}(\omega)$ is zero up to a gap frequency 2Δ, above which it rises monotonically to the frequency-independent conductivity of the normal state σ_n, since ω is still much smaller than τ^{-1}. Since most of oscillator strength remains at finite frequencies, the sphere resonance linewidth would not change at all.

In the other normal-state limit where $\omega_p\tau\sim 1$, there is no observable sphere resonance in the normal state since

$$\mathrm{Re}[\epsilon(\omega_{sr})+2\epsilon_h]>0 .$$

However, the $\delta(\omega)$ term in $\sigma_{1s}(\omega)$ in the superconducting state will make $\epsilon_{1s}(\omega)$ negatively diverging at low frequency by the Kramers-Kronig relation.[25] Therefore, a sphere resonance will occur upon cooling through the transition as long as

$$\mathrm{Im}[\epsilon(\omega_{sr})+2\epsilon_h]\ll 1 .$$

If $2\Delta\tau>1$ (Case III), a resonance appears in the superconducting state since $\sigma_{1s}(\omega)$ is zero at all finite frequencies so $\mathrm{Im}[\epsilon(\omega_{sr})+2\epsilon_h]$ is always zero. If $2\Delta\tau\ll 1$ and $\omega_{sr}<2\Delta$ (Case IV), the resonance appears since $\mathrm{Im}[\epsilon(\omega_{sr})+2\epsilon_h]$ is zero below the gap energy. However, if $2\Delta\tau\ll 1$ and $\omega_{sr}\gg 2\Delta$ (Case V), then the real part of the optical conductivity above 2Δ will make the resonance overdamped.

The important property of the small particle geometry for superconductors is that it can be used to translate the δ function associated with the conductivity of the superconducting condensate from zero frequency to finite frequency where it can be inspected with spectroscopic methods. Since the strength of the δ function is closely related to the London penetration depth,[26] the sphere resonance in principle provides information about this dc property. Therefore by studying the characteristics of the sphere resonance (the strength, position, and linewidth), we identify some important features of the carrier electrodynamics as well as the minimum possible energy gap for various high-T_c superconductors.

None of the Cu oxide superconductors we have studied have a far-infrared resonance (fir) feature in the normal state. However, a sphere resonance is found in superconducting $La_{2-x}Sr_xCuO_{4-y}$, $Nd_{1.85}Ce_{0.15}CuO_4$, and $Bi_4Ca_3Sr_3Cu_4O_z$ but not in $YBa_2Cu_3O_{7-y}$ particles. An analysis based on the Maxwell-Garnett formalism[27] demonstrates that the resonance is polarized along the c axis. Lack of the resonant feature in the normal state indicates that at the resonance frequency the normal-state carriers along the c axis are in the classical limit, $|\epsilon_1-\epsilon_0|<\epsilon_2$, where ϵ_0 describes the low-frequency contribution from phonon and interband transitions. The simi-

TABLE I. The characteristics of sphere resonances in superconducting materials with various relative values of ω_p, τ, and 2Δ. The dielectric constant ϵ_0 is from excitations above the sphere resonance frequency, i.e., phonons and bound electrons.

Case	Conditions	Peak position, ω_{sr}	Observable? (normal)	(s.c.)	Characteristics
I	$\omega_p\tau\gg 1$, $(2\Delta)\tau>1$	$\dfrac{\omega_p}{(\epsilon_0+2\epsilon_h)^{1/2}}$	Yes	Yes	The linewidth narrows upon cooling below T_c, since all of the oscillator strength goes to a zero-frequency δ function.
II	$\omega_p\tau\gg 1$, $(2\Delta)\tau\ll 1$	$\dfrac{\omega_p}{(\epsilon_0+2\epsilon_h)^{1/2}}$	Yes	Yes	The linewidth will not change upon cooling below T_c, since most of the oscillator strength remains above the gap.
III	$\omega_p\tau\leq 2$, $(2\Delta)\tau>1$	$\dfrac{\omega_p}{(\epsilon_0+2\epsilon_h)^{1/2}}$	No	Yes	The peak will shift down in frequency as the temperature is raised because the area of the δ function decreases.
IV	$\omega_p\tau\leq 2$, $(2\Delta)\tau\ll 1$, and $\omega_{sr}<2\Delta$	$\left[\dfrac{16\sigma_n(2\Delta)}{\epsilon_0+2\epsilon_h}\right]^{1/2}$	No	Yes	The peak position will have the same temperature dependence as that of $(2\Delta)^{1/2}$.
V	$\omega_p\tau\leq 2$, $(2\Delta)\tau\ll 1$, and $\omega_{sr}\gg 2\Delta$	$\left[\dfrac{16\sigma_n(2\Delta)}{\epsilon_0+2\epsilon_h}\right]^{1/2}$	No	No	The peak cannot be seen since $\mathrm{Im}[\epsilon(\omega_{sr})+2\epsilon_h]$ is large for either state.

larity of the sphere resonances observed for these p-type and n-type systems indicates that the Drude parameters for the c-axis response must be nearly the same.

The $La_{2-x}Sr_xCuO_{4-y}$ system has been studied in the most detail. The results are that the frequency and strength of this resonant mode increase with increased Sr doping x, decrease with applied magnetic field, and decrease as the temperature is raised; the resonance disappears above the superconducting transition temperature. However, except for the $x=0.15$ sample, the temperature dependence of the resonance position cannot be described in terms of the Mattis-Bardeen theory. The disappearance of the resonance in samples with $x>0.2$ puts a lower bound of the c-axis energy gap of $3.0\ k_BT_c$. A preliminary report of some of these results has already been published.[19]

In the next section, our experimental results, including sample preparation and measurement techniques, are discussed. Then the temperature dependence, Sr concentration, and magnetic field dependence of the observed resonant absorption feature for $La_{2-x}Sr_xCuO_{4-y}$ are described in detail. The temperature-dependent results for $Nd_{1.85}Ce_{0.15}CuO_4$ and $Bi_4Ca_3Sr_3Cu_4O_z$ are also shown. In Sec. III, we derive analytical expressions for the position and strength of a sphere resonance in superconducting particles. Next the phonon contributions and effects of anisotropy are introduced. A comparison of theory and experiment for $La_{2-x}Sr_xCuO_{4-y}$ is presented in Sec. IV. Several important aspects of the resonance are discussed in Sec. V. Possible mechanisms for the large background absorption and the line broadening, which cannot be explained by a phonon-coupling model, are presented. Finally, we summarize our findings in Sec. VI.

II. EXPERIMENTAL RESULTS

A. Sample preparation and characterization techniques

The series of polycrystalline samples of $La_{2-x}Sr_xCuO_{4-y}$ used in this experiment were prepared by solid-state reaction of $SrCO_3$, CuO, and La_2O_3. The well-mixed powders are ground and fired in air. The fired powder is reground and refired, typically two times, until the material becomes single phase, as determined by x-ray diffraction. This material is pressed into pellets, fired at 1050 °C for 12 h in a flowing O_2 atmosphere, and slowly cooled to 500 °C. After being annealed for 5 h at 500 °C, the pellets are slowly cooled to room temperature. X-ray diffraction measurements confirm that our samples are single phase. The dc resistivity measured using the conventional four-probe technique yielded transition temperatures for the various values of x in good agreement with published data[28] (Table II).

Having been characterized in bulk pellet form, the pellets were ground into a fine powder using a methanol slurry which was then mixed with 0.6-μm Teflon powder in volume fractions f from 0.3% to 3%. These mixtures of Teflon and oxide powder were then vacuum dried and pressed into pellets 13 mm in diameter and 2 mm thick. The mixed powder was observed under a scanning electron microscope (SEM) and found to consist of particles

TABLE II. Characteristics of resonances for the series of $La_{2-x}Sr_xCuO_{4-y}$ samples. The resonant frequency ω_{sr}, the normalized peak absorptivity $\alpha(\omega_{sr})/f$, and the normalized integrated absorption strength, I/f are given.

x	T_c [a] (K)	f	ω_{sr} (cm^{-1})	$\alpha(\omega_{sr})/f$ (cm^{-1})	I/f (cm^{-2})
0.02		0.03			
0.04		0.03			
0.08	28	0.03	12.0	89	600
0.10	31	0.03	18.7	165	1 800
0.12	32	0.03	23.0	196	2 500
0.15	37	0.01	53.7	602	12 500
0.18	35	0.003	75.1	643	20 000
0.20	31	0.003	87.7	490	20 000
0.225	14	0.003			
0.25	10	0.003			

[a]Zero resistance temperature.

~ 2 μm in diameter well dispersed in the Teflon. Figure 3(a) shows an SEM picture of one of our samples. The solid line indicates 10 μm. In Fig. 3(b) we show the electron diffraction pattern of one of the isolated particles. The uniformity of the pattern demonstrates that the particle is a single crystal. About 80% of the particles are single crystals and most of the remainder are bicrystals.

B. Far-infrared measurements

Far-infrared normal incidence transmission spectra were measured using lamellar grating (2–40 cm^{-1}) and Michelson (10–200 cm^{-1}) interferometers in conjunction with 0.3-K He^3-cooled Ge bolometric detectors. The samples were held in light pipes which could be rotated in and out of the light path, allowing the raw transmission spectrum T (sample) to be ratioed to that of a pure Teflon pellet, T (Teflon). The sample temperature could

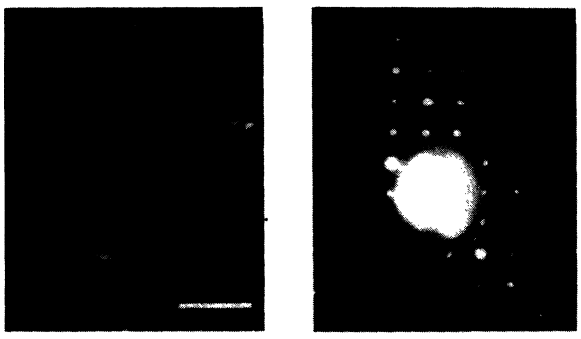

FIG. 3. (a) An SEM picture of 1 mol% $La_{1.8}Sr_{0.2}CuO_{4-y}$ particles in Teflon. The solid bar in the figure indicates 10 μm. The photograph shows that the particles are well separated. (b) The electron diffraction pattern of a typical $La_{1.8}Sr_{0.2}CuO_{4-y}$ particle in the Teflon matrix. This TEM picture shows that the particle is composed of one single crystal. The diffuse scattering is from the Teflon. About 80% of the particles are single crystals, and the remainder are bicrystals.

be varied between 4 and 70 K, and was monitored with a carbon resistor thermometer. The absorption coefficient α was obtained from the following equation:

$$\alpha = -\frac{1}{t}\ln\frac{T\ (\text{sample})}{T\ (\text{Teflon})}\ ,$$

where t is the sample thickness.

To measure the magnetic field dependence, a cryostat with a superconducting magnet was used. To reduce the thermal coupling between the sample and the detector, the sample holder was wrapped with aluminized Mylar and placed inside an evacuable chamber. Transmission spectra were measured at various magnetic fields at a given temperature between 1.4 and 40 K. In this configuration, there is no reference pellet, so only the difference between the absorption coefficients in different magnetic fields can be obtained.

1. *Temperature dependence of the absorption features*

The temperature dependence of α for 1 mol% $La_{1.85}Sr_{0.15}CuO_{4-y}$ in Teflon is shown in Fig. 4(a). These data have been corrected for the change in detector sensitivity produced by the difference in thermal loading between the sample and reference which produces a shift of $\Delta\alpha \sim 1.0$ in the ordinate of Fig. 4(a). A strongly temperature-dependent resonant feature is seen at temperature below 40 K but the spectrum remains almost constant from 40 to 70 K. The disappearance of this peak above T_c indicates that the feature is closely connected with superconductivity even though the larger absorption does occur in the superconducting state. To clearly show the temperature dependence of the absorption peak, we plot the difference between $\alpha(T)$ and $\alpha(T=40\ \text{K})$ in Fig. 4(b). The absorption peak, located around 54 cm^{-1} at 4 K, remains almost constant at low temperature, but moves to lower frequency as the temperature approaches T_c and the strength weakens. Similar temperature dependence is observed for $La_{2-x}Sr_xCuO_{4-y}$ samples with $x \leq 0.18$. Figures 5 and 6 show the temperature dependence of the absorption coefficients for $La_{1.92}Sr_{0.08}CuO_{4-y}$ and $La_{1.90}Sr_{0.10}CuO_{4-y}$, respectively.

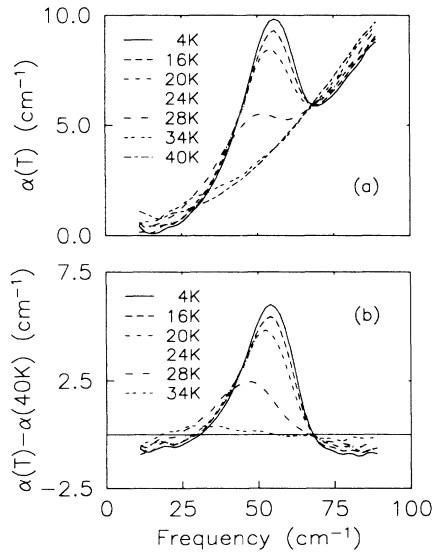

FIG. 4. Temperature dependence of the absorption coefficient α for 1% $La_{1.85}Sr_{0.15}CuO_{4-y}$ particles in Telfon. (a) Absorption coefficient and (b) difference between α in the superconducting and normal states.

Of the eight superconducting samples of different doping the temperature-dependent resonance described above is characteristic of five, while of the three remaining samples ($x \geq 0.2$) two do not show a resonance and the third is shown in Fig. 7. This sample, which has the highest-frequency sphere mode which has been observed, consists of 0.3% volume fraction $La_{1.8}Sr_{0.2}CuO_{4-y}$ in Teflon. As the temperature approaches T_c, the peak is observed to weaken, but to remain at almost the same frequency. This temperature dependence is similar to the observation of Schlesinger *et al.*[20] in their $La_{1.80}Sr_{0.20}CuO_{4-y}$ powder sample.

2. *Sr concentration dependence of the absorption feature*

Figure 8 shows the temperature dependence of the normalized sphere resonance frequency for the six different Sr dopings. Even though the peak positions of most of the samples decrease as T approaches T_c, the normalized behavior does not fall onto one universal curve. There is a big difference between samples with $x < 0.15$ and those with $x \geq 0.15$. The curves in this figure show the various limits of the BCS theory, which will be discussed later along with the London penetration depth, λ.

Figure 9(a) shows the ratio of the normalized integrated absorption strength to the sphere resonance frequency, versus resonance frequency. The open circles are the

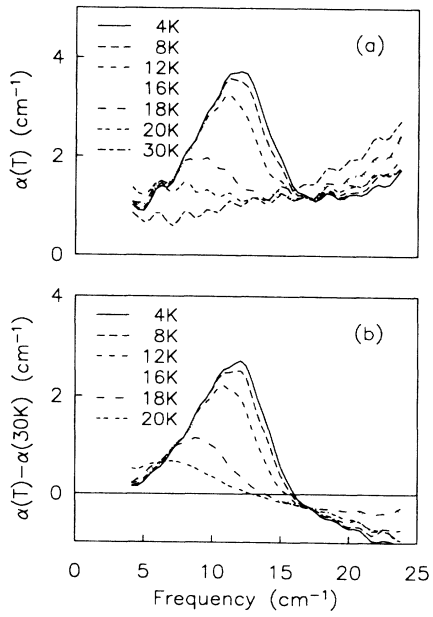

FIG. 5. Temperature dependence of the absorption coefficient α for 3% $La_{1.92}Sr_{0.08}CuO_{4-y}$ particles in Teflon. (a) Absorption coefficient and (b) difference between α in the superconducting and normal states.

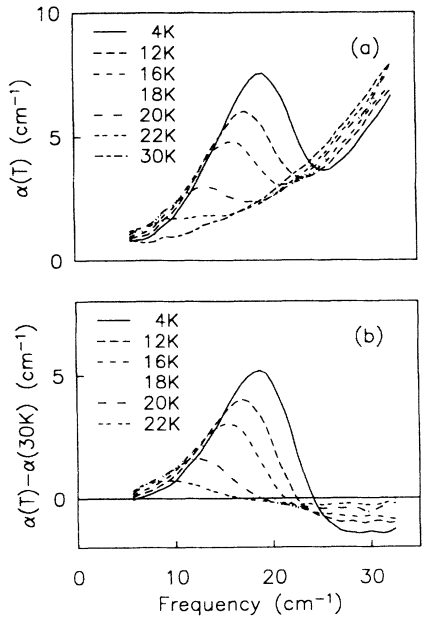

FIG. 6. Temperature dependence of the absorption coefficient α for 3% $La_{1.90}Sr_{0.10}CuO_{4-y}$ particles in Teflon. (a) Absorption coefficient and (b) difference between α in the superconducting and normal states.

data. This figure shows that the integrated absorption strength is approximately proportional to the square of the resonance frequency. Figure 9(b) shows the ratio of the FWHM to the sphere resonance frequency (open triangles), which is nearly constant for most of the samples. (Detailed information about the absorption peaks for

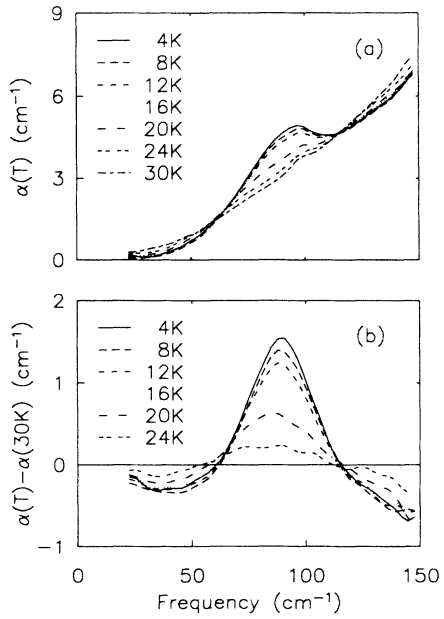

FIG. 7. Temperature dependence of the absorption coefficient α for 0.3% $La_{1.80}Sr_{0.20}CuO_{4-y}$ particles in Teflon. (a) Absorption coefficient and (b) difference between α in the superconducting and normal states. The resonant frequency remains fairly constant as the temperature is raised.

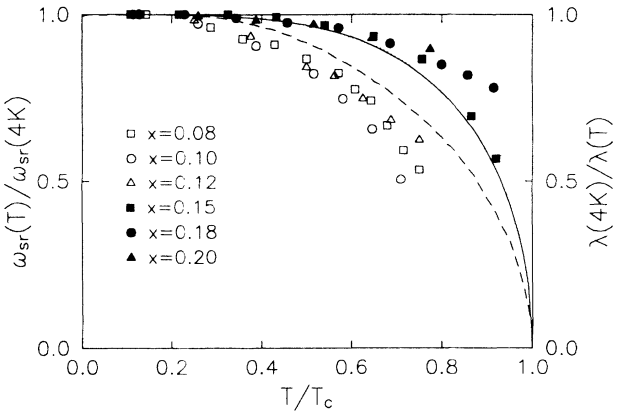

FIG. 8. Normalized sphere resonance frequency squared vs reduced temperature for the six different $La_{2-x}Sr_xCuO_{4-y}$ samples which show absorption peaks. The dotted line is the theoretical prediction of $\omega_{sr}(T)/\omega_{sr}(4\text{ K})$ for $La_{1.85}Sr_{0.15}CuO_{4-y}$. For other samples, our theory based on the Mattis-Bardeen equation predicts curves almost identical to the dotted line, which does not agree with the data. Since $\omega_{sr}(T)/\omega_{sr}(4\text{ K})$ is the same as $\lambda(4\text{ K})/\lambda(T)$, we can compare our experimental data with various limits of the BCS predictions. The solid line and the dashed line show the BCS predictions in two extreme limits: the extreme anomalous limit and the local clean limit, respectively.

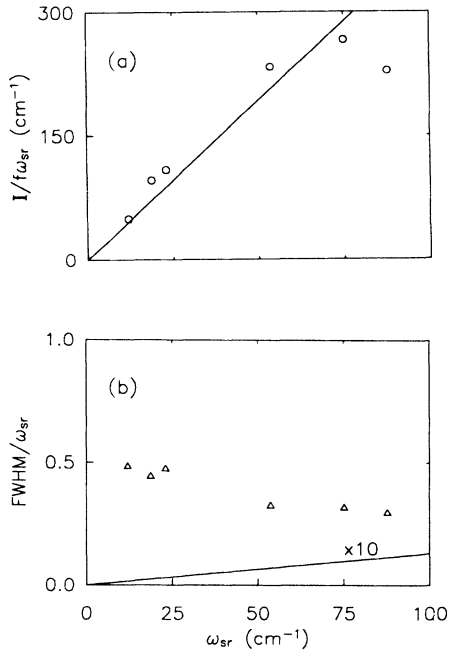

FIG. 9. (a) Normalized integrated absorption strength divided by the sphere resonance frequency, vs resonance frequency, for the six superconducting samples which show absorption peaks. The open circles are the data, and the solid line indicates the theoretical prediction described in the text. (b) Full width at half maximum (FWHM) divided by resonance frequency, vs resonance frequency. The open triangles are the data and the solid line is the theoretical prediction, multiplied by 10.

various Sr concentrations is shown in Table II.) The solid line in each figure is the theoretical prediction based on the interaction between the free carrier and photon sphere resonance modes.

3. *Magnetic field dependence of the absorption features*

Figure 10 shows the difference between the absorption coefficient at 5 different magnetic fields and that at 6 T for the 3 mol% $La_{1.92}Sr_{0.08}CuO_{4-y}$ sample and the 3 mol% $La_{1.90}Sr_{0.10}CuO_{4-y}$ sample. (The sample temperature for this measurement is 1.4 K.) The maximum difference in absorption coefficients between 0 and 6 T is a significant fraction of the difference between the superconducting and normal-state values in zero field. Note that $\Delta\alpha_{max}$ in Fig. 10(a) is about 2, compared to $\Delta\alpha(\omega_{sr})=2.6$ in Fig. 5(b) for the $x=0.08$ sample. This comparison indicates that a significant portion of the resonance strength disappears by 6 T. Moreover, the difference in absorption coefficients between 0 and 6 T has a derivative form indicating that the peak position is shifting to a lower frequency as the magnetic field is applied. We conclude that the effect on the resonance of increasing magnetic field is similar to that of raising the temperature.

4. *Other Cu oxide materials*

We have investigated the sphere resonance in various Cu oxide materials including the nonsuperconducting copper oxides $La_2SrCu_2O_{6+\delta}$ and $La_4BaCu_5O_{13}$. Studies of the nonsuperconducting but metallic copper oxides were included since these materials share some physical properties with the high-T_c superconductors; for example, these nonsuperconducting materials have a linear temperature dependence in the conductivity[29] and an apparent infrared conductivity peak if the reflectivity of the sintered sample is measured and used for Kramers-Kronig transformation.[30] However, the absorption coefficient of these nonsuperconducting materials shows almost no temperature dependence in our measured frequency region. This observation illustrates that the sphere resonance feature is not a general property of metallic copper oxide but is solely related to superconductivity.

We have also studied the far-infrared absorptivity of various other superconducting particles. We have found superconducting sphere resonances in small isolated particles of $Nd_{1.85}Ce_{0.15}CuO_{4-y}$ and $Bi_4Ca_3Sr_3Cu_4O_z$ in Teflon. Figure 11 shows the temperature dependence of α for 3 mol% $Nd_{1.85}Ce_{0.15}CuO_{4-y}$ particles in Teflon. This material exhibits a strong line at about 7 cm^{-1} which shifts down in frequency as the temperature approaches T_c, similar to the temperature dependence of α in the $La_{2-x}Sr_xCuO_{4-y}$ samples. Unlike $La_{2-x}Sr_xCuO_{4-y}$, the charge carriers for $Nd_{1.85}Ce_{0.15}CuO_{4-y}$ are known to be electrons.[31] However, the similar characteristics of the sphere resonance for the p-type and n-type systems indicate that the electrodynamic parameters of carriers responsible for resonance should be nearly identical. Figure 12 shows the temperature dependence of the absorption coefficient for 10 mol% $Bi_4Ca_3Sr_3Cu_4O_z$ particles in Teflon. As shown in Fig. 12(a), the background absorption in the superconducting state is quite large in this material. In order to see the resonance one must subtract the normal-state absorptivity, as in Fig. 12(b). Evident here is a very broad feature at about 10 cm^{-1} which disappears as the temperature is raised above T_c.

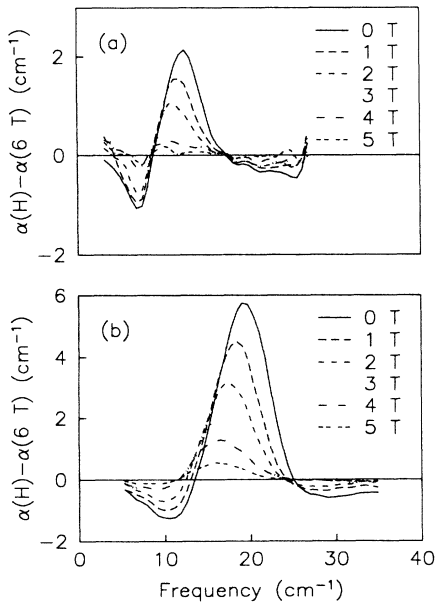

FIG. 10. Magnetic field dependence of the absorption features in (a) $La_{1.92}Sr_{0.08}CuO_{4-y}$ and (b) $La_{1.90}Sr_{0.10}CuO_{4-y}$. The sample temperature is 1.2 K. The difference between the absorption coefficients at 5 different fields and that at 6 T is plotted. The effect of the magnetic field is qualitatively similar to that of raising the temperature.

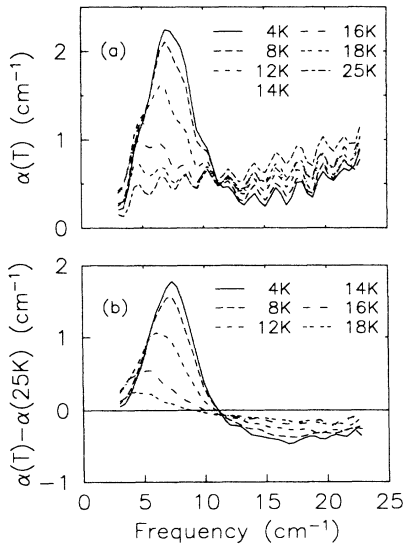

FIG. 11. Temperature dependence of the absorption coefficient α for 3% $Nd_{1.85}Ce_{0.15}CuO_{4-y}$ particles in Teflon. (a) Absorption coefficient and (b) difference between α in the superconducting and normal states. Measured $T_c=23$ K.

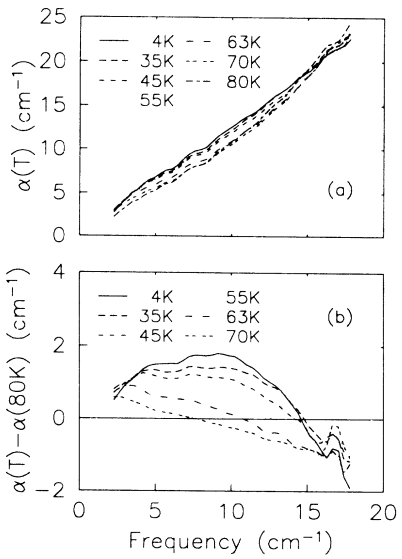

FIG. 12. Temperature dependence of the absorption coefficient α for 3% $Bi_4Ca_3Sr_3Cu_4O_z$ particles in Teflon. (a) Absorption coefficient and (b) difference between α in the superconducting and normal states. Measured $T_c \sim 80$ K.

For the $YBa_2Cu_3O_{7-y}$ samples, particles were imbedded in either Teflon or CsI. (CsI was used to get the spectrum above 180 cm^{-1}, where Teflon is highly absorbing.) In the frequency region below the lowest phonon, $YBa_2Cu_3O_{7-y}$ particles show smaller absorption in the superconducting state than in the normal state, in agreement with the observed frequency behavior far away from the sphere resonance frequency in $La_{2-x}Sr_xCuO_{4-y}$ particles. Also, the difference between the superconducting-state and normal-state absorptivity decreases as the temperature approaches T_c or as a magnetic field is applied. However, due to the very complicated phonon spectrum that appeared above 135 cm^{-1}, we could not identify an obvious superconducting sphere resonance for this material.

III. THEORY

Many physical properties of inhomogeneous media[32] are well described in terms of an effective dielectric constant, which usually depends on the dielectric constants and the volume fractions of each constituent. The validity of using an effective dielectric constant instead of local dielectric constants depends on two size conditions: first, for each particle, the size must be large enough so that a macroscopic dielectric constant can be defined; second, the particle size must be small compared to the wavelength of the radiation in the medium. For our isolated superconducting particles, these two conditions are satisfied.

A. Maxwell-Garnett approximation

1. Isotropic particles

Historically, the first effective dielectric function was the Maxwell-Garnett (MG) expression,[27] which is an application of the Clausius-Mossotti relation[23] to polarizable spherical particles embedded in a dielectric host, whose dielectric constant is ϵ_h. The Clausius-Mossotti relation is:[23]

$$\frac{\epsilon^{av}-\epsilon_h}{\epsilon^{av}+2\epsilon_h}=\frac{4\pi}{3}n\alpha_p \ , \tag{3}$$

where ϵ^{av} is the effective dielectric constant and n is the number density of particles in the medium. From Eq. (1), the polarizability, α_p, can be written as

$$\alpha_p=\frac{\epsilon(\omega)-\epsilon_h}{\epsilon(\omega)+2\epsilon_h}a^3 \ . \tag{4}$$

By inserting Eq. (4) into Eq. (3), we can get an equation for ϵ^{av},

$$\frac{\epsilon^{av}-\epsilon_h}{\epsilon^{av}+2\epsilon_h}=f\frac{\epsilon(\omega)-\epsilon_h}{\epsilon(\omega)+2\epsilon_h} \tag{5}$$

with

$$f=\frac{4\pi}{3}na^3 \tag{6}$$

defining the volume fraction of spheres. Equation (5) can be solved to obtain

$$\epsilon^{av}=\epsilon_h\frac{2(1-f)\epsilon_h+(1+2f)\epsilon(\omega)}{(2+f)\epsilon_h+(1-f)\epsilon(\omega)} \ . \tag{7}$$

This Maxwell-Garnett expression has been successfully applied to many dilute systems[32] of small metal particles embedded in insulating host materials.

2. Anisotropic particles

If the dielectric constant of the sphere is anisotropic, each component of the polarizability along the principal axes has the form of Eq. (4). We perform an angle average[33] to obtain the isotropic ϵ^{av}:

$$\frac{\epsilon^{av}-\epsilon_h}{\epsilon^{av}+2\epsilon_h}=\frac{f}{3}\sum_i\frac{\epsilon_j(\omega)-\epsilon_h}{\epsilon_j(\omega)+2\epsilon_h} \ , \tag{8}$$

where j indicates the crystal axis. If $\epsilon_a \approx \epsilon_b (=\epsilon_{ab})$, as is the case with this high-T_c superconductor, then Eq. (8) can be written as

$$\frac{\epsilon^{av}-\epsilon_h}{\epsilon^{av}+2\epsilon_h}=\frac{f}{3}\left[2\frac{\epsilon_{ab}-\epsilon_h}{\epsilon_{ab}+2\epsilon_h}+\frac{\epsilon_c-\epsilon_h}{\epsilon_c+2\epsilon_h}\right] \ . \tag{9}$$

B. Sphere resonances

In order to obtain analytical expressions for the sphere resonance in isolated superconducting particles, we begin with the isotropic Maxwell-Garnett theory (MG), i.e., Eq. (7), applied to superconducting carriers. (The optical properties of normal-state particles have been described in some detail by Genzel and Martin.[22]) These considerations lead to the consideration of superconducting carriers plus optic phonons. A generalization to anisotropic

particles is given in Sec. III B 3. Finally, the contribution from the magnetic dipole absorption is examined.

1. *Superconducting particles*

The concept of an energy gap separating the superconducting ground state from excited states has been used to explain many properties of conventional superconductors.[34] For most conventional superconductors, the gap energy 2Δ is much smaller than τ^{-1}, so the normal-state conductivity near 2Δ is a constant value equal to σ_n, as shown in Fig. 2(b). In this extreme dirty limit[16] ($2\Delta \ll \tau^{-1}$), $\sigma_1(\omega)$ at zero temperature is zero up to a gap frequency 2Δ, above which it rises monotonically to the conductivity of the normal state, σ_n. Define $\int \sigma_1(\omega)d\omega = S$, the oscillator strength. The difference of the oscillator strengths between the normal and superconducting states appears at zero frequency in the superconducting state. The strength of the $\delta(\omega)$ term A at zero temperature in $\sigma_{1s}(\omega)$ is[25]

$$A = \int_{0^+}^{\infty} (\sigma_{1n} - \sigma_{1s}) d\omega \approx 2\sigma_n(2\Delta), \quad \text{if } 2\Delta \ll \tau^{-1} . \tag{10}$$

This equation shows that A is determined by the plasma frequency ω_p, the scattering rate τ^{-1} of the normal-state carriers, and the superconducting gap value.

For the high-T_c superconducting materials, it has been suggested by some[14] that the clean limit, i.e., ($2\Delta \gg \tau^{-1}$), should be applied. In this case, the entire Drude conductivity component is located at frequencies below 2Δ, so it collapses to zero frequency upon cooling. The zero-temperature strength of the resulting $\delta(\omega)$ term can be evaluated directly from the sum rule[24] for free carriers:

$$\begin{aligned} A &= \int_{0^+}^{\infty} (\sigma_{1n} - \sigma_{1s}) d\omega \\ &= \int_{0^+}^{\infty} \sigma_{1n} d\omega = \frac{\omega_p^2}{8}, \quad \text{if } 2\Delta \gg \tau^{-1} . \end{aligned} \tag{11}$$

In this limit A is independent of the scattering rate of the normal-state carriers and the gap value.

In either case the $\delta(\omega)$ term in $\sigma_1(\omega)$ produces a $1/\omega$ dependence in $\sigma_2(\omega)$ as seen from a Kramers-Kronig relation:[25]

$$\begin{aligned} \sigma_2^A &= -\frac{2\omega}{\pi} \int_0^{\infty} \frac{\sigma_1^A(\omega')}{\omega'^2 - \omega^2} d\omega' \\ &= -\frac{2\omega}{\pi} \int_0^{\infty} \frac{A\delta(\omega')}{\omega'^2 - \omega^2} d\omega' = \frac{2A}{\pi\omega} . \end{aligned} \tag{12}$$

Using Eq. (12), the dielectric response of the superconducting state below the energy gap can be written as

$$\begin{aligned} \epsilon_s(\omega) &\cong \left[\epsilon_\infty - \frac{8A}{\omega^2} \right] + i\frac{4\pi A\delta(\omega)}{\omega} \\ &= \lim_{1/\tau_s \to 0} \left[\epsilon_\infty - \frac{8A}{\omega(\omega + i/\tau_s)} \right] . \end{aligned} \tag{13}$$

In the clean limit, Eq. (13) is always valid since $\sigma_1(\omega) = 0$ at finite frequencies. However, in the extreme dirty limit, Eq. (13) cannot be used above the gap value due to the finite conductivity.

To obtain the effective dielectric response of superconducting particles in the host medium, Eq. (13) is inserted into Eq. (7) and the result takes the Lorentz form

$$\epsilon^{\text{av}}(\omega) = \epsilon_\infty^{\text{av}} \lim_{1/\tau_s \to 0} \left[\frac{\omega_{Le}^2 - \omega^2 - i\omega/\tau_s}{\omega_e^2 - \omega^2 - i\omega/\tau_s} \right] , \tag{14}$$

where

$$\omega_{Le}^2 = \frac{8A}{\epsilon_\infty} \frac{\epsilon_\infty(1+2f)}{\epsilon_\infty(1+2f) + 2\epsilon_h(1-f)} \tag{15}$$

and

$$\omega_e^2 = \frac{8A}{\epsilon_\infty} \frac{\epsilon_\infty(1-f)}{\epsilon_\infty(1-f) + \epsilon_h(2+f)} . \tag{16}$$

The parameter $\epsilon_\infty^{\text{av}}$ is the high-frequency limit of Eq. (7).

The sphere resonance frequency of Eq. (14) is

$$\begin{aligned} \omega_{\text{sr}} = \omega_e &= \left[\frac{8A}{\epsilon_\infty} \frac{\epsilon_\infty(1-f)}{\epsilon_\infty(1-f) + \epsilon_h(2+f)} \right]^{1/2} \\ &\approx \left[\frac{8A}{\epsilon_\infty + 2\epsilon_h} \right]^{1/2} \quad \text{in the limit } f \ll 1 . \end{aligned} \tag{17}$$

Since the damping of the resonance in Eq. (14) determined by $1/\tau_s$ vanishes in the superconducting state, $\sigma^{\text{av}}(\omega)$ of the isolated particles becomes a δ function at the resonant frequency:

$$\begin{aligned} \sigma^{\text{av}}(\omega) &= \frac{\omega}{4\pi} \lim_{1/\tau_s \to 0} \text{Im}[\epsilon^{\text{av}}(\omega)] \\ &= \frac{\epsilon_\infty^{\text{av}}(\omega_{Le}^2 - \omega_e^2)}{4\pi} \lim_{1/\tau_s \to 0} \left[\frac{\omega^2/\tau_s}{(\omega_e^2 - \omega^2)^2 + (\omega/\tau_s)^2} \right] \\ &= \frac{\epsilon_\infty^{\text{av}}}{8} (\omega_{Le}^2 - \omega_e^2) \delta(\omega - \omega_e) . \end{aligned} \tag{18}$$

In the dilute limit, the strength of the δ-function term of $\sigma^{\text{av}}(\omega)$ can be approximated as

$$\begin{aligned} S = \int_0^{\infty} \sigma^{\text{av}}(\omega) d\omega &= \frac{\epsilon_\infty^{\text{av}}}{8} (\omega_{Le}^2 - \omega_e^2) \\ &\approx \frac{9\epsilon_h^2}{(\epsilon_\infty + 2\epsilon_h)^2} Af \quad \text{with } f \ll 1 . \end{aligned} \tag{19}$$

Thus, in the dilute limit, the strength of the sphere resonances depends linearly upon f in agreement with our experimental observations.

2. *Interaction with phonons*

The dielectric response of the superconducting state, Eq. (13), can be modified to include the contribution of phonons by adding a Lorentz term:

$$\begin{aligned} \epsilon_s(\omega) &\cong \epsilon_\infty \frac{\omega_{\text{LO}}^2 - \omega^2 - i\gamma\omega}{\omega_{\text{TO}}^2 - \omega^2 - i\gamma\omega} - \frac{8A}{\omega^2} + i\frac{4\pi A\delta(\omega)}{\omega} \\ &= \epsilon_\infty \lim_{1/\tau_s \to 0} \left[1 - \frac{(8A/\epsilon_\infty)}{\omega(\omega + i\omega/\tau_s)} + \frac{\omega_{\text{LO}}^2 - \omega_{\text{TO}}^2}{\omega_{\text{TO}}^2 - \omega^2 - i\gamma\omega} \right] , \end{aligned} \tag{20}$$

where ω_{TO} and ω_{LO} are TO and LO mode frequencies, and γ is the damping constant for the TO phonon. If there is more than one IR active phonon and the sphere resonance is below the lowest-frequency mode, then Eq. (20) is still a good approximation, assuming that ω_{TO} and ω_{LO} are TO and LO mode frequencies of the lowest-lying phonon and that ϵ_∞ contains the residues of the higher-lying phonons.

By inserting Eq. (20) into Eq. (7), we can obtain the effective dielectric response[22] of this more complex system:

$$\epsilon^{av}(\omega)=\epsilon_\infty^{av}\frac{(\omega^2-\omega_{L+}^2)(\omega^2-\omega_{L-}^2)+i\omega\Delta(\omega)}{(\omega^2-\omega_+^2)(\omega^2-\omega_-^2)+i\omega\Gamma(\omega)}\ , \tag{21}$$

where

$$\omega_\pm^2=\frac{\omega_{ph}^2+\omega_e^2}{2}\pm\left[\left[\frac{\omega_{ph}^2+\omega_e^2}{2}\right]^2-\omega_e^2\omega_{TO}^2\right]^{1/2}\ , \tag{22}$$

$$\omega_{L\pm}^2=\frac{\omega_{Lph}^2+\omega_{Le}^2}{2}\pm\left[\left[\frac{\omega_{Lph}^2+\omega_{Le}^2}{2}\right]^2-\omega_{Le}^2\omega_{TO}^2\right]^{1/2}\ , \tag{23}$$

$$\Gamma(\omega)=\gamma(\omega^2-\omega_e^2)\ , \tag{24}$$

$$\Delta(\omega)=\gamma(\omega^2-\omega_{Le}^2)\ , \tag{25}$$

$$\omega_{ph}^2=\omega_{TO}^2\frac{\epsilon_0(1-f)+\epsilon_h(2+f)}{\epsilon_\infty(1-f)+\epsilon_h(2+f)}\ , \tag{26}$$

$$\omega_{Lph}^2=\omega_{TO}^2\frac{\epsilon_0(1+2f)+2\epsilon_h(1-f)}{\epsilon_\infty(1+2f)+2\epsilon_h(1-f)}\ , \tag{27}$$

and

$$\epsilon_0=\epsilon_\infty\left[\frac{\omega_{LO}}{\omega_{TO}}\right]^2\ . \tag{28}$$

Equation (21) gives rise to two sphere resonances, at frequencies ω_+ and ω_-, which can be understood by examining Fig. 13. Figure 13(a) shows the two components of the real part of the dielectric function. If we look at the sphere resonance condition on each of the dielectric components the resonances occur at ω_e and ω_{ph}. For the coupled system with the two resonances well separated the correct resonant frequencies are not far removed from these approximate values as shown in Fig. 13(b). Figure 13(c) shows the two resonances in the conductivity of the effective medium. In our experiment, the observed

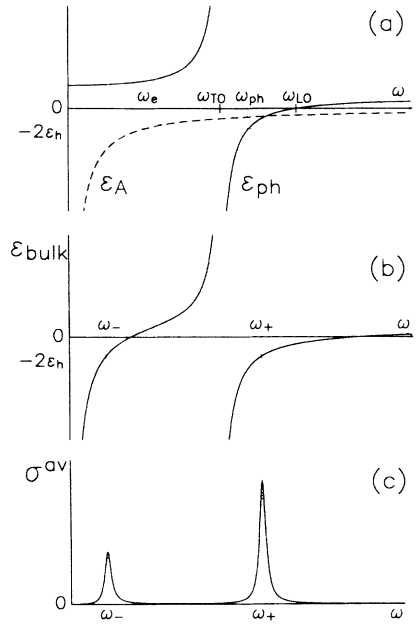

FIG. 13. The dielectric response function for the bulk and composite form of a material with phonon and superconducting condensate contributions included. (a) Contributions to the real part of the bulk dielectric function of the phonon (ϵ_{ph}) and that of the superconducting condensate (ϵ_A). (b) The total real part of the bulk dielectric function. (c) The effective conductivity of a small particle of this material. Note that the two zero crossings of the real part of the dielectric function of the bulk material give rise to two peaks in the imaginary part of the dielectric function of the isolated particles.

resonance occurs well below ω_{TO}, and thus coincides with ω_-.

Figure 14 shows the dependence of the resonant frequencies ω_+ and ω_- upon $\sqrt{8A}$. For $A=0$, there is only the resonance at ω_+, associated with the zero crossing of the bulk dielectric constant due to the phonon. For small values of $\sqrt{8A}$, the resonance at ω_- has the characteristics of the superconducting sphere resonance without any phonons, while the resonance at ω_+ follows ω_{ph}, which is the phonon sphere resonance frequency of a pure ionic material without free carriers. For large values of $\sqrt{8A}$, the resonance at ω_- asymptotically approaches ω_{TO}, while the higher resonant frequency ω_+ approaches ω_e. This behavior can be derived from Eq. (22) in two limiting cases:

$$\left.\begin{aligned}\omega_-\approx\omega_{TO}\left[\frac{\omega_e}{\omega_{ph}}\right]&\rightarrow\left[\frac{8A}{(\epsilon_0+2\epsilon_h)}\right]^{1/2}\\ \omega_+\approx\omega_{ph}&\rightarrow\omega_{TO}\left[\frac{\epsilon_0+2\epsilon_h}{\epsilon_\infty+2\epsilon_h}\right]^{1/2}\end{aligned}\right\}\ \text{if}\ \left[\frac{8A}{\epsilon_\infty}\right]^{1/2}\ll\omega_{TO},\omega_{LO}\ , \tag{29}$$

and

$$\left.\begin{aligned}\omega_-&\approx\omega_{TO}\\ \omega_+\approx\omega_e&\rightarrow\left[\frac{8A}{(\epsilon_\infty+2\epsilon_h)}\right]^{1/2}\end{aligned}\right\}\ \text{if}\ \left[\frac{8A}{\epsilon_\infty}\right]^{1/2}\gg\omega_{TO},\omega_{LO}\ . \tag{30}$$

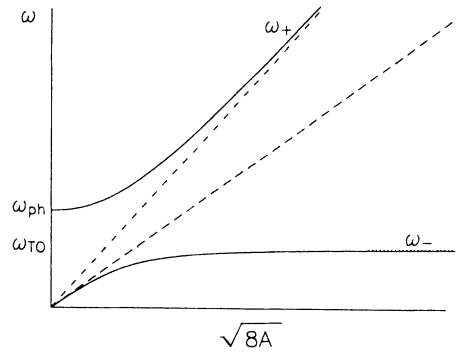

FIG. 14. The dependence of the two resonant frequencies, ω_+ and ω_-, upon $\sqrt{8A}$. For small carrier density, ω_- is roughly proportional to $\sqrt{8A}$. The dashed line is the behavior of ω_- in Eq. (29) and the dash-dotted line is the behavior of ω_+ in Eq. (30).

Since our observed sphere resonance is well below $\omega_{\rm TO}$, $\omega_{\rm sr}$ corresponds to ω_- in the limit of $\sqrt{8A/\epsilon_\infty} \ll \omega_{\rm TO}$.

We have not been able to obtain an analytical formula for the integrated area of the sphere resonance if the phonon contribution is included; however, in the limit of $\sqrt{8A/\epsilon_\infty} \ll$ or $\gg \omega_{\rm TO}$, the resonance should have the characteristic of superconducting carriers while the phonon response is represented by ϵ_0 or ϵ_∞. Therefore, the limiting strengths for the ω_- mode (S_-) and the ω_+ mode (S_+) are[35]

$$S_- \approx \frac{9\epsilon_h^2}{(\epsilon_0+2\epsilon_h)^2} Af \quad \text{if} \quad \left[\frac{8A}{\epsilon_\infty}\right]^{1/2} \ll \omega_{\rm TO}, \omega_{\rm LO} , \tag{31a}$$

$$S_+ \approx \frac{9\epsilon_h^2}{(\epsilon_\infty+2\epsilon_h)^2} Af \quad \text{if} \quad \left[\frac{8A}{\epsilon_\infty}\right]^{1/2} \gg \omega_{\rm TO}, \omega_{\rm LO} . \tag{31b}$$

The conductivity of the effective medium at the peak position can be evaluated from Eq. (21),

$$\sigma^{\rm av}(\omega=\omega_{\rm sr}) = \frac{1}{4\pi}\{\omega_- {\rm Im}[\epsilon^{\rm av}(\omega_0)]\} = -\frac{\epsilon_\infty^{\rm av}(\omega_-^2-\omega_{L+}^2)(\omega_-^2-\omega_{L-}^2)}{4\pi\gamma(\omega_-^2-\omega_{Le}^2)} . \tag{32}$$

In the limit of $\sqrt{8A/\epsilon_\infty} \ll \omega_{\rm TO}$ and $f \ll 1$,

$$\sigma^{\rm av}(\omega=\omega_{\rm sr}) \approx \frac{9\epsilon_h^2}{\epsilon_0}\frac{1}{\gamma}\frac{\omega_{\rm LO}^2\omega_{\rm TO}^2}{(\omega_{\rm LO}^2-\omega_{\rm TO}^2)} f . \tag{33}$$

This equation shows that the conductivity of the sphere resonance is no longer a δ function and that the peak value is independent of A. Even though ω_- is much smaller than $\omega_{\rm TO}$, so that the resonant response has the characteristic of free superconducting carriers, the resonance is broadened by the coupling to the TO phonon. This can be seen by calculating the linewidth from Eqs. (31) and (33):

$$\Delta\Gamma \approx \frac{(\epsilon_0-\epsilon_\infty)}{(\epsilon_0+2\epsilon_h)^2}\frac{A}{\omega_{\rm TO}^2}\gamma \approx \frac{\gamma}{8}\left[\frac{\epsilon_0-\epsilon_\infty}{\epsilon_0+2\epsilon_h}\right]\left[\frac{\omega_-}{\omega_{\rm TO}}\right]^2 . \tag{34}$$

Equation (34) shows that the linewidth is proportional to the TO phonon damping constant γ, the optical activity of the TO mode, and the resonance frequency squared.

3. *Effects of conductivity anisotropy on the sphere resonance*

Since most high-T_c superconductors have anisotropic dielectric constants,[6,11] the effect of the anisotropy on the low-frequency sphere resonance will be treated by using the anisotropic form of the MG, i.e., Eq. (9) with the low-frequency contribution to the phonons represented by ϵ_0. With the assumption that the sphere resonance occurs in the *ab* plane, the effective dielectric function has the same form as Eq. (14) with modified ω_{Le} and ω_e. The peak occurs at

$$\omega_{\rm sr} \approx \omega_e = \left[\frac{8A}{\epsilon_{0ab}}\frac{\epsilon_{0ab}[1-(1+B)p]}{\epsilon_{0ab}[1-(1+B)p]+\epsilon_h[2+(1-2B)p]}\right]^{1/2} \rightarrow \left[\frac{8A}{\epsilon_{0ab}+2\epsilon_h}\right]^{1/2} \tag{35}$$

and the strength of the resonance in the dilute limit is

$$S \approx \frac{9\epsilon_h^2}{(\epsilon_{0ab}+2\epsilon_h)^2} Ap = \frac{9\epsilon_h^2}{(\epsilon_{0ab}+2\epsilon_h)^2} A\tfrac{2}{3}f , \tag{36}$$

where ϵ_{0ab} is the dc dielectric constant in the *ab* plane and

$$B = \frac{1}{2}\frac{\epsilon_c-\epsilon_h}{\epsilon_c+2\epsilon_h} \quad \text{and} \quad p = \tfrac{2}{3}f .$$

By comparing Eqs. (34) and (35) with Eqs. (17) and (19), one can see that the resonance occurs at the same frequency and the strength of the resonance is about $\frac{2}{3}$ that of the isotropic medium. (If the sphere resonance occurs along the *c* axis, a similar analysis shows that the strength is reduced by a factor of 3 with respect to the isotropic case.)

4. *Magnetic dipole absorption*

In small particles, induced eddy currents produce nonzero magnetization even though the bulk material is not magnetic.[36] These currents can make a significant contribution in the far-infrared called magnetic dipole absorption.[37] The average magnetic permeability, $\mu_{\rm av}$, of a collection of spheres of a material with an isotropic dielectric constant has a form similar to Eq. (7):

$$\mu_{\rm av} = \frac{2(1-f)+(1+2f)\mu_m}{(2+f)+(1-f)\mu_m} , \tag{37}$$

where μ_m is the permeability of a uniformly magnetized sphere in the alternating magnetic field. For isotropic particles, μ_m can be written in terms of the spherical Bessel functions $j_0(\kappa a)$ and $j_2(\kappa a)$:[36]

$$\mu_m = \frac{2j_0(\kappa a)+2j_a(\kappa a)}{2j_0(\kappa a)+j_2(\kappa a)} , \tag{38}$$

where κ is the wave vector of the radiation inside the conducting particle. For a sphere with an anisotropic dielectric constant, we are not aware of any analytical expression for $\mu_{\rm av}$. However, if the *ab* plane conductivity is much larger than the *c*-axis value (as is the case with high-T_c superconductors), the magnetic dipole absorption will be dominated by the eddy current contribution induced in the *ab* plane, where the varying magnetic field is pointing along the *c* axis. Therefore, for randomly oriented particles, the magnetic dipole absorption is expected to be $\frac{1}{3}$ the magnetic dipole absorption for isotropic particles whose dielectric constant is the same as that of the *ab* plane.

For $f \ll 1$ and $a \ll \delta$, where δ is the skin depth, a low frequency of expansion[37] of the isotropic MG gives

$$\alpha = \frac{2\omega}{c}\mathrm{Im}(\epsilon_{\rm av}\mu_{\rm av})^{1/2} \approx f\frac{\omega^2}{c^2}\sqrt{\epsilon_h}\left[\frac{9c\epsilon_h}{4\pi\sigma}+\frac{2\pi}{5c}a^2\sigma\right] , \tag{39}$$

where σ is the conductivity of the particles. The first term corresponds to the electric dipole absorption and the second term to the magnetic dipole contribution. For superconducting particles, $\sigma_1(\omega)$ is zero below the energy gap, so there is no magnetic dipole contribution in this frequency region. For a sphere resonance below the energy gap, the magnetic dipole absorption does not change the absorption in the superconducting state but does increase the absorption in the normal state.

IV. COMPARISON OF THEORY AND EXPERIMENT

The analytic expressions developed in the previous section are zero-temperature results and provide only limited checks on the data since the position and strength of the sphere resonance depends both on the temperature and on the carrier concentration. In order to cover the full spectrum of data numerical work must be included. First, using the La_2CuO_{4-y} single-crystal data of Schlesinger *et al.*,[11] we have obtained values for the phonon LO and TO modes and widths, as well as values for ϵ_∞ in the *ab* plane and along the *c* axis, from fitting the reflectivity with the standard factored form of the dielectric function of Bassat *et al.*:[38]

$$\epsilon_j = \epsilon_{\infty j}\prod_x \frac{\omega_{xj\rm LO}^2-\omega^2-i\gamma_{xj}\omega}{\omega_{xj\rm TO}^2-\omega^2-i\gamma_{xj}\omega} - \frac{\omega_{pj}^2}{\omega(\omega+i\gamma_{pj})} , \tag{40}$$

where j indicates the crystal axis. The derived values for these parameters, shown in Table III, can then be used in the anisotropic MG to describe the response of the small particles. The mode frequencies are left fixed but the values of $\epsilon_{\infty j}$ are allowed to change because of the possibility of higher electronic states induced by Sr doping. Then, the superconducting response is modeled by numerical integration with the temperature-dependent Mattis-Bardeen equations.[16]

Our experimental data together with the known properties of the sintered material provide important constraints on the parameters used to model the resonance.

(1) The resonance does not appear in the normal state, as shown in Fig. 4. As explained in the Introduction, its absence in the normal state indicates that the charge car-

TABLE III. Classical oscillator parameters of the $(La,Sr)_2CuO_{4-y}$ system. Upper: Phonons obtained from the La_2CuO_{4-y} data of Schlesinger *et al.*[11] The *ab*-plane Drude parameters obtained by Tajima *et al.*[9] from the reflectivity of $La_{1.85}Sr_{0.15}CuO_{4-y}$ single crystals. Middle: The 1% $La_{1.85}Sr_{0.15}CuO_{4-y}$ in Teflon composite data of this work with the sphere resonance direction in the *ab*-plane. Lower: Same as middle, but directed along the *c* axis.

	$\omega_{\rm TO}$ ($\rm cm^{-1}$)	$\omega_{\rm LO}$ ($\rm cm^{-1}$)	γ ($\rm cm^{-1}$)	ϵ_∞	σ_0 ($\Omega^{-1}\,\rm cm^{-1}$)
ab plane	135	245	55	7.0	900
	360	455	40		
	650	670	20		
c axis	242	465	100	4.5	0
	494	560	24		
ab plane	135	245	55	3.2	13
	360	455	40		
	650	670	20		
c axis	242	465	100	4.5	0
	494	560	24		
ab plane	135	245	55	7.0	900
	360	455	40		
	650	670	20		
c axis	242	465	100	3.0	7.2
	494	560	24		

riers which participate in the sphere resonance in the superconducting state are heavily damped in the normal state, i.e., $|\epsilon_1(\omega_s)| \ll \epsilon_2(\omega_s)$.

(2) There is no sphere resonance in samples with $x > 0.2$ even though they are superconducting. This is only possible in Case V in Table I, so the carriers in $La_{2-x}Sr_xCuO_{4-y}$ follow the limit of $1/\tau > 2\Delta$.

(3) As shown in Eqs. (29) and (31a), the resonance position and its strength depend only on A and ϵ_0. Therefore, if the resonance position and its strength are measured, A and ϵ_0 are uniquely determined. In our coupled sphere mode theory, measurement of the linewidth provides additional information about the phonon damping constant as shown in Eq. (34); however, we found that the measured linewidth is too broad to be explained by the phonon coupling mechanism within the original Mattis-Bardeen equation. Therefore, in our numerical simulation, we have ignored the measured linewidth and instead focused our attention on the resonant frequency and line strength as the physically significant parameters. The large linewidth probably indicates that other broadening mechanisms are important for $La_{2-x}Sr_xCuO_{4-y}$, and we will take up this problem in Sec. V E.

A. *ab*-plane or *c*-axis resonance?

The experimental data for the $x=0.15$ sample is shown in Fig. 15. The anisotropic form of the MG described in Eq. (9) does not mix the *ab*-plane and *c*-axis dielectric responses; therefore, the data may be associated with one of two possibilities, either a sphere resonance in the *ab* plane or one along the *c* axis. Let us first consider the *ab* plane.

The predicted behavior of the $x=0.15$ sample using values of ω_{pab}, τ_{ab}, and $\epsilon_{\infty ab}$ from the single-crystal study of Tajima *et al.*[9] is shown in Fig. 15(a). The single-crystal values of these parameters do not produce a sphere resonance, since the predicted peak position is much larger than the gap value so $\mathrm{Im}[\epsilon(\omega_{sr})]$ is not negligible (Case V in Table I).

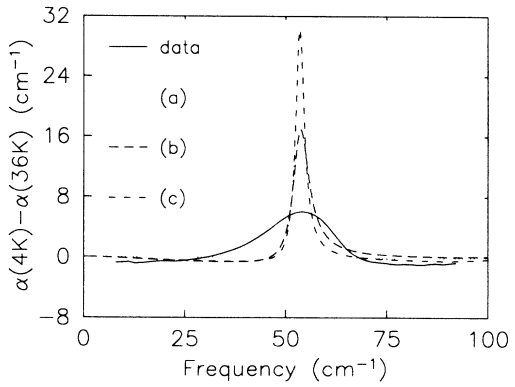

FIG. 15. Calculated fits to the sphere resonance in $La_{1.85}Sr_{0.15}CuO_{4-y}$ for the three sets of parameters given in Table II, along with the experimental result. (a) The single crystal parameters of Tajima *et al.*,[9] (b) fitting the sphere resonance in the *ab* plane, and (c) along the *c* axis. In the latter two cases the fit was done by matching the center frequency and the integrated absorption strength of the experimental resonance.

In Fig. 15(b) we show that a fit can be obtained by changing significantly the values of ω_{pab}, τ_{ab}, and $\epsilon_{\infty ab}$ but the resultant parameters are unreasonable. In this fit, we adjust the values of σ_{nab} and $\epsilon_{\infty ab}$ in order to match both the center frequency and integrated absorption strength of the experimental absorption feature. The values of the parameters used in this fit are given in Table III. Even though the *ab*-plane fit can qualitatively describe the resonance, the problem with this approach is that a very small value of σ_{nab} must be used in order to match the position and the strength of the peak. The position and the strength are related to $A \approx 2\sigma_{nab}(2\Delta_{ab})$ and ϵ_{0ab} as shown in Eqs. (29) and (31) so the observed peak position and the strength uniquely determine the values of A and ϵ_{0ab}. Assuming $2\Delta_{ab}=3.5\ k_BT_c$, the fit requires a small value of σ_{nab} of about 13 $\Omega^{-1}\,\mathrm{cm}^{-1}$, which is about 150 times smaller than the reported dc value[28] of sintered $La_{1.85}Sr_{0.15}CuO_4$ and 70 times smaller than the *ab*-plane value[9] for single crystals in the fir region. Therefore, it is more plausible to assume that the sphere resonance is polarized along the *c* axis, in which direction the carrier density is expected to be very small.

Our calculated fit to the $x=0.15$ sample using a *c*-axis sphere resonance is shown in Fig. 15(c). The parameters which provide the best fit to the data with $2\Delta_c=3.5k_BT_c$ are given in Table III. The value of σ_{nc} used in this fit is about 7.2 $\Omega^{-1}\,\mathrm{cm}^{-1}$, which implies an anisotropy ratio between the *ab*-plane and *c*-axis conductivities of about 100, a value consistent with dc measurements on $La_{2-x}Sr_xCuO_{4-y}$,[39] and $YBa_2Cu_3O_{7-y}$,[15] but much smaller than the measured value of $Bi_2Sr_2CaCu_2O_8$ single crystals.[40] This value is also consistent with the lower bound[11] of 50 for the fir anisotropy ratio of $La_{2-x}Sr_xCuO_{4-y}$.

Additional evidence that the sphere resonance is polarized along the *c* axis is provided by our magnetic field measurements. H_{c2} has been measured for $La_{2-x}Sr_xCuO_{4-y}$ single crystals[39] and been found to be highly anisotropic: At 4 K, the value of H_{c2} with the magnetic field along the *c* axis is about 12 T, whereas with the magnetic field in the *ab* plane it is already 20 T at 15 K and increases dramatically at lower temperatures, becoming unmeasurably large. Therefore, if the resonance is polarized in the *ab* plane, our applied magnetic field is negligible compared to H_{c2}, so there would be very little magnetic field dependence. (This argument agrees with the weak magnetic field dependence of the reflectivity of sintered $La_{1.85}Sr_{0.15}CuO_{4-y}$ observed by other workers.[41]) The large magnetic field dependence of our resonance is only consistent with the magnetic field dependence of the dc resistivity if the resonance is polarized along the *c* axis.

This *c*-axis resonance picture is also consistent with the sphere resonances observed in other superconducting Cu oxide particles. In Case IV of Table I (which applies to $La_{2-x}Sr_xCuO_{4-y}$), the resonance position is about

$$[16\sigma_n(2\Delta)/(\epsilon_0+2\epsilon_h)]^{1/2}\ .$$

Assuming that $2\Delta=3.5\ k_BT_c$ and $\epsilon_0+2\epsilon_h=25$, the mea-

sured c-axis conductivity value,[40] 0.072 $\Omega^{-1}\,cm^{-1}$, for $Bi_4(Sr,Ca)_6Cu_4O_y$ single crystals predicts a sphere resonance along the c axis at 7 cm^{-1} in good agreement with our measured value, 9 cm^{-1}. For $Nd_{1.85}Ce_{0.15}CuO_{4-y}$, the measured conductivity from the sintered pellet[31] is about 30 Ω^{-1} cm^{-1}. Since $Nd_{1.85}Ce_{0.15}CuO_{4-y}$ has a crystal structure similar to that of $La_{2-x}Sr_xCuO_{4-y}$, it is reasonable to assume that its anisotropy ratio is also 100. These values predict a c-axis sphere resonance at 7 cm^{-1}, consistent with the measured sphere resonance position of the same value. Therefore, we can conclude that the superconducting resonances in $La_{2-x}Sr_xCuO_{4-y}$, $Bi_4Sr_3Ca_3Cu_4O_y$, and $Nd_{1.85}Ce_{0.15}CuO_{4-y}$ are all polarized along the c axis.

B. Temperature dependence

Figure 16 shows the calculated absorption coefficient versus temperature for $La_{1.85}Sr_{0.15}CuO_{4-y}$. Similar to our experimental observation in Sec. II B 1, our model based on the Mattis-Bardeen theory predicts that the resonance position moves to lower frequency and its strength weakens as T approaches T_c. The temperature dependence of the predicted peak position is plotted as a dotted line in Fig. 8. and agrees well with the experimental observation. We made fits to the other samples and found that their dependence is almost identical to the theoretical prediction for the $x=0.15$ sample: This does not agree with our experimental observation. Therefore, the excellent agreement between our measured peak position and the theoretical prediction for the $x=0.15$ sample may not be a general finding.

In addition, our model cannot explain two important aspects of the experimental data: The large linewidth and the background absorption. A comparison of Fig. 16(a) with the experimental data in Fig. 4(a) shows that the weak temperature dependence of the background absorption appears in the model but the magnitude of the calculated effect is too small. Moreover, the predicted linewidth is much smaller than the experimental value. In our model, the background absorption and the line broadening come from the absorption tail produced by the damping of the TO phonon. Therefore, the strong discrepancy in the background absorption and the line broadening must stem from another mechanism. Possible mechanisms for the background absorption and the line broadening will be discussed in Sec. V D and V E.

C. Effects of Sr doping

We now show that the change in the peak position and strength as a function of Sr concentration can be explained as a change in the value of σ_{nc}. A numerical calculation for different σ_{nc}'s is plotted in Fig. 17(a). As σ_{nc} increases, the peak position and the strength, $I=\int\alpha(\omega)d\omega$, increase as predicted by Eqs. (29) and (31). Figure 17(a) also shows that for large c-axis conductivity the resonance finally starts to broaden and disappear above 2Δ. Above the energy-gap frequency, the remaining conductivity is big enough that the second resonance condition in Eq. (2) is not satisfied, so the resonance cannot be observed. The measured normalized absorption coefficients for various Sr doping concentrations are plotted in Fig. 17(b). If we increase the Sr doping concentration, the number of mobile carriers increases, hence the conductivity also increases. Therefore, the peak position

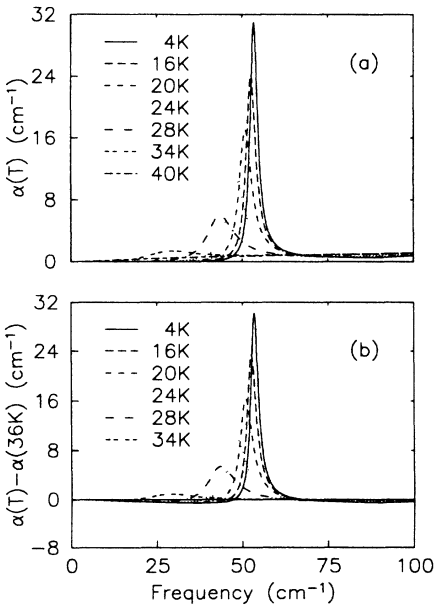

FIG. 16. Theoretical predictions for the c-axis sphere resonance fit described in the text for the $x=0.15$ sample. (a) Absorption coefficient and (b) difference between α in the superconducting and normal states.

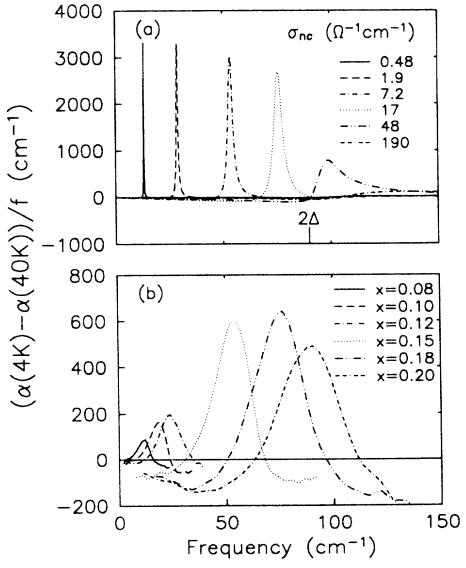

FIG. 17. (a) Effect of changing the conductivity in the sphere resonance model. The peak height remains constant but the width decreases as the resonance moves to lower frequency, away from the phonon. For higher values of the conductivity, the resonance broadens and disappears above the gap. (b) Experimental results for six different Sr dopings x. The resonance disappears above $x=0.2$.

and its line strength should increase with Sr doping. If x becomes bigger than 0.2, the predicted peak position becomes larger than the gap value so the sphere resonance disappears (Case V of Table I).

The Sr doping study provides a test of the c-axis sphere resonance model. The line strength I, of the resonance feature can be written as

$$I=\int \alpha\, d\omega=\int 4\pi\omega\, \mathrm{Im}(\sqrt{\epsilon})d\omega\approx\int \frac{8\pi^2\sigma}{\sqrt{\epsilon}}d\omega\approx\frac{8\pi^2}{\sqrt{\epsilon_h}}S\ . \tag{41}$$

As shown in Sec. III B 3, the conductivity anisotropy brings out a factor of $\frac{1}{3}$ for the c-axis resonance. Using Eqs. (29) and (31a), we get a relationship between I and ω_{sr}:

$$I\approx\frac{1}{3}\frac{8\pi^2}{\sqrt{\epsilon_h}}S\approx\frac{3\pi^2\epsilon_h\sqrt{\epsilon_h}}{(\epsilon_{0c}+2\epsilon_h)}\omega_{sr}^2 f\ . \tag{42}$$

This is a simple relationship between I and ω_{sr} which depends only on the value of ϵ_{0c}. Using the single-crystal value of $\epsilon_{0c}=22$, Eq. (42) predicts a straight line for $I/f\omega_{sr}$ vs ω_{sr}, shown by the solid line in Fig. 9(a). This parameter independent fit is in excellent agreement with most of the experimental data. The deviation for the largest frequency may be a consequence of the resonance approaching the gap frequency.

As mentioned in Sec. IV C, the predicted linewidth is too small compared to the experimental value. In our phonon-coupling model, the linewidth is controlled by the damping coefficient of the lowest-lying TO phonon mode as shown in Eq. (34). The prediction of Eq. (34) is plotted as a solid line in Fig. 9(b). This predicted value is more than an order of magnitude too small. Moreover, the measured FWHM divided by ω_{sr} is almost independent of ω_{sr}, which is not consistent with the linear relationship produced by our phonon-coupling model. This discrepancy must be explained by the presence of broadening mechanisms other than TO phonon coupling.

V. DISCUSSION

A. Isotropic model versus anisotropic model

The fir sphere resonance in superconducting $La_{1.85}Sr_{0.15}CuO_{4-y}$ particles can also be modeled with the isotropic Maxwell-Garnett expression, using the same isotropic dielectric function ϵ_{eff} that is measured for sintered samples. This coincidence occurs since ϵ_{eff} of $La_{1.85}Sr_{0.15}CuO_{4-y}$ has the characteristics of the ab-plane plasmonlike behavior in the superconducting state mixed with the strong c-axis phonon, as shown by Sulewski *et al.*[6] In this section, we want to present experimental evidence which shows that the simple isotropic model cannot be used to explain our superconducting sphere resonance.[42,43]

The most important and direct experimental evidence against the isotropic model is that most of the particles are actually single crystallites. As shown in the SEM picture of Fig. 3(a), the particles are well isolated and their typical size is about 2 μm, which is much smaller than the original grain size in the sintered ceramic (about 10 μm). Moreover, the electron diffraction pattern in Fig. 3(b) shows that most individual particles are single crystallites. Since the particles used in our experiments are well-separated single crystallites, we have no choice but to use the anisotropic form of the single-crystal dielectric function.

Secondly, the isotropic model does not give a consistent description of the observed magnetic field dependence. It has been shown by Sulewski[41] that the low temperature fir response of sintered $La_{1.85}Sr_{0.15}CuO_{4-y}$ ($T_c=37$ K) is nearly independent of magnetic field up to 8.5 T. Therefore, if the isotropic dielectric function measured for sintered samples is used, this isotropic model should predict that the sphere resonance is almost independent of magnetic field. Our magnetic field measurements on samples with $x=0.10$ ($T_c=31$ K) and $x=0.15$ ($T_c=37$ K) at 1.2 K, shown in Fig. 18(a) and 18(b), display a strong magnetic field dependence with the resonance nearly quenched at 6 T in the first case and strongly modified in the second. For comparison, the supernormal temperature induced change in the resonance at both Sr concentrations is represented by the solid trace.

Models which include explicitly the anisotropic nature of $La_{2-x}Sr_xCuO_{4-y}$ can explain the magnetic field dependence of the sintered materials as well as that of the small particles. As shown in Sec. IV A, our c-axis polarized sphere resonance model is consistent with the measured magnetic field dependence of the c-axis conductivity. For the sintered material, Sulewski *et al.*[6] already showed that its response is well modeled with the free-carrier-type response in the ab plane and the strong c-axis phonon. Since the ab-plane conductivity shows a weak

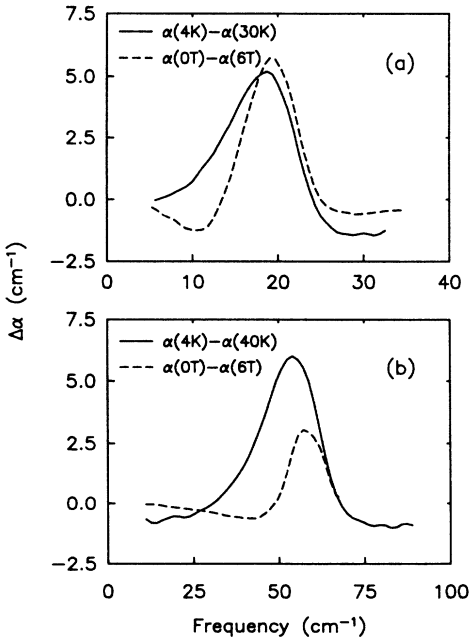

FIG. 18. Comparison of the magnetic field and temperature dependence of the sphere resonance for two Sr concentrations. (a) $La_{1.90}Sr_{0.10}CuO_{4-y}$. (b) $La_{1.85}Sr_{0.15}CuO_{4-y}$.

dependence on magnetic field,[39] the fir response of sintered $La_{2-x}Sr_xCuO_{4-y}$ should and does show the same weak magnetic field dependence.

Finally, the conductivity required to explain the sphere resonance is in good agreement with the *c*-axis dc conductivity value as shown in Sec. IV A. For $La_{2-x}Sr_xCuO_{4-y}$ and $Nd_{1.85}Ce_{0.15}CuO_{4-y}$, the required conductivities are smaller than the *ab*-plane dc values by two orders of magnitude. For the $Bi_4Sr_3Ca_3Cu_4O_y$ case, the conductivity required to explain the sphere resonance is about five orders of magnitude smaller than the dc value in the *ab* plane.

B. Estimate of the gap energy

The observation of the sphere resonance puts a lower limit on the *c*-axis gap value. Since according to Fig. 17(a) the resonance disappears rapidly as the gap value is crossed from below, a lower bound on the gap occurs when $\omega_s = 2\Delta_c$. According to the experimental data in Table II, the peak value of the resonance decreases when x is changed from 0.18 to 0.20 similar to the change seen in Fig. 17 between curves labelled $\sigma_n = 17$ and 48 ($\Omega^{-1}\text{cm}^{-1}$) that correspond to a resonance slightly below or above the gap. Taking the lower value to obtain a lower bound we find that $2\Delta_c/k_BT_c \geq 3.0$. This value is a more stringent bound than the limit given in Ref. 15 of Ref. 19. Some recent theoretical models, such as some resonating-valence-bond (RVB) models,[44] in which the gap is reported to be $\sim 0.2\ k_BT_c$ are not consistent with our observation of a sphere resonance. If $2\Delta_c = 0.2\ k_BT_c$, our observed peak at about 75 cm^{-1} is much higher than the gap value of about 6 cm^{-1}, so the resonance could not be observed (Case V of Table I).

C. London penetration depth

One of the important phenomenological parameters describing the nature of superconductivity is the London penetration depth λ which represents the penetration depth of the dc magnetic field inside a superconducting sample.[26] Through the dependence on the superconducting energy gap, the temperature dependence of λ is related fundamentally to the symmetry of the superconducting state, and thus to the pairing mechanism.[45,46] Furthermore, the zero-temperature value $\lambda(0)$ contains information on the effective mass and the density of the superconducting carriers n_s, which is proportional to the strength A of the bulk conductivity δ function. The penetration depth can be written as

$$\lambda^{-2} = 4\pi n_s e^2/(mc^2) = 8A/c^2 . \tag{43}$$

From Eq. (31a), we can show that

$$\lambda = \frac{c}{\sqrt{8A}} \approx \frac{1}{\sqrt{\epsilon_0 + 2\epsilon_h}} \frac{c}{\omega_{\text{sr}}} . \tag{44}$$

This equation shows that a measurement of the sphere resonance position and ϵ_0 can determine the London penetration depth.

There have been numerous reports on the magnitude and temperature dependence of λ in various high-T_c superconductors, especially $YBa_2Cu_3O_{7-y}$, obtained by various techniques, such as magnetic susceptibility,[45] muon-spin-resonance (μSR) techniques,[46,47] polarized neutron reflection,[48] and radio frequency penetration depth.[49] These experiments are very sensitive to the sample quality, such as surface barriers, defects, or flux trapping, and significant disagreements exist among the reported values.[50] Moreover, most of the reported values are limited to the *ab* plane. However, Eq. (44) suggests a new method to measure λ, i.e., a measurement of the sphere resonance frequency. As we demonstrated in Sec. IV A, the observed fir sphere resonance is polarized along the *c* axis. Therefore, careful studies of the sphere resonance in various oxide superconductors can provide information about the London penetration depth along the *c* axis.

Inspection of Eq. (44) and Table II shows that the *c*-axis penetration depth, λ_c, decreases as the doping concentration increases. Contrary to the early observation[46] that T_c is proportional to λ_{ab}^{-2} for $YBa_2Cu_3O_{7-y}$, a simple relation between T_c and λ_c for $La_{2-x}Sr_xCuO_{4-y}$ does not appear. With the single-crystal value[11] of $\epsilon_{0c} = 22$ and $\omega_{\text{sr}} = 53.7$ cm^{-1} for $La_{1.85}Sr_{0.15}CuO_4$, Eq. (44) gives $\lambda_c(0) = 5.8$ μm. This value is much larger than the value of $\lambda_{ab}(0) \approx 0.3$ μm measured by other techniques.[46]

Now, let us turn to consider the penetration depth in $Yba_2Cu_3O_{7-y}$. As we mentioned in Sec. II B 4, the fir response of $YBa_2Cu_3O_{7-y}$ particles below 135 cm^{-1} agrees with the expected behavior away from the resonance. Above 135 cm^{-1}, we could not observe any obvious superconducting resonance due to the complicated phonon spectrum. From these observations, the predicted sphere resonance position can be argued to be larger than 135 cm^{-1}. If we assume a similar value of ϵ_{0c}, then Eq. (44) gives an upper bound of 2.3 μm for $\lambda_c(0)$ in $YBa_2Cu_3O_{7-y}$. This value is in good agreement with other experimental estimates,[45,47] and much larger than the value $\lambda_{ab}(0) \approx 0.15$ μm measured by other techniques. Since n_s is inversely proportional to λ^2, the large value of $\lambda_c(0)$ for the various oxide superconductors indicates that the density of the superconducting carrier along the *c* axis is very small.

The normalized temperature dependence of the *c* axis London penetration depth for various Sr doping concentrations is shown in Fig. 8. For the $x = 0.15$ sample, the temperature dependence of the *c*-axis London penetration depth follows the prediction (solid line) of the empirical "two-fluid" approximation;[26] i.e.,

$$\lambda(0)/\lambda(T) = [1 - (T/T_c)^4]^{1/2} .$$

This observation is also in good agreement with the temperature dependence of the *ab* plane $\lambda(T)$ for $La_{1.85}Sr_{0.15}CuO_4$ measured by μSR techniques. Similar behavior has been also observed for the *ab* plane $\lambda(T)$ in $YBa_2Cu_3O_{7-y}$ by both μSR techniques[46,47] and magnetic susceptibility studies.[45] This temperature dependence of $\lambda(T)$ for $La_{1.85}Sr_{0.15}CuO_4$ and $YBa_2Cu_3O_{7-y}$ has been interpreted as evidence for a BCS (*s*-wave) superconductor by many workers.[46,47] This conclusion of *s*-wave cou-

pling is different from that of some specific-heat measurements.[51]

The behavior of the empirical "two-fluid" model is very close to the BCS prediction for $\lambda(T)$ in the extreme anomalous limit, i.e., $\xi_0/\lambda(0)\rightarrow\infty$. Considering the extremely small value of coherence length ξ_0 for the oxide superconductors, it is evident that $\lambda(0)/\lambda(T)$ for the oxide superconductor should follow the behavior of the local limit [$\xi_0/\lambda(0)=0$] instead of that of the extreme anomalous limit. In the clean local limit [$\xi_0/\lambda(0)=0$ and $\ell \gg \xi_0$, where ℓ is the mean free path of the free carriers], $\lambda(0)/\lambda(T)$ starts to decrease at much lower temperature as shown by the dashed line in Fig. 8. In the dirty local limit [$\xi_0/\lambda(0)=0$ and $\ell \ll \xi_0$], the temperature dependence of the penetration depth is located between the above-mentioned extreme limits.

Figure 8 shows that the temperature dependence of $\lambda(0)/\lambda(T)$ decreases as the Sr doping concentration increases. Except for the $x=0.15$ sample, the temperature dependence of $\lambda(0)/\lambda(T)$ does not follow any of the various BCS limits. Moreover, there is a clear difference between the behavior of $\lambda(0)/\lambda(T)$ in $x>0.15$ samples and that in $x<0.15$ samples. For the $x>0.15$ sample, $\lambda(0)/\lambda(T)$ has weaker temperature dependence than that of the extreme anomalous limit. On the other hand, for the $x<0.15$ samples, $\lambda(0)/\lambda(T)$ decreases much faster than the prediction of the clean local limit. The source of these systematic differences needs to be understood.

D. Possible mechanisms for the background absorption

A comparison of Figs. 4(a) and 16(a) shows that our observed normal-state absorption coefficient is larger than the calculated one by one order of magnitude. Moreover, the predicted temperature dependence of the absorption coefficient above ω_{sr} is too small to explain the data. This indicates that other absorption mechanisms are important. We can divide the possible mechanisms into two groups, intrinsic and extrinsic.

Three possible candidates for intrinsic absorption mechanisms are: (1) interband transition, (2) enhanced electric field in the Teflon, and (3) magnetic dipole absorption.

(1) The absorption tail of an overdamped interband transition can contribute to the background absorption just like the phonon tail. Putting in the known values from the literature[5] of the strength, center frequency and linewidth of the midband absorption observed for sintered $La_{1.85}Sr_{0.15}CuO_{4-y}$, we find that this term is an order of magnitude too small to account for the background absorption observed in the sphere resonance configuration.

(2) Between the highly conducting particles, the electric field in the host material is enhanced. This effect has been shown to produce a big enhancement of the background absorption if the host material is highly absorbing like gelatin.[52] However, due to the small fir absorption coefficient of Teflon, this effect is negligible in our case.

(3) Another intrinsic absorption mechanism is magnetic dipole absorption. Figure 19 shows calculated absorption coefficients α for the superconducting and normal states, with and without magnetic dipole contribution. When only the electric dipole absorption is included, curves (a) and (b) are obtained for the superconducting and normal states, respectively. However, as discussed in Sec. III B 4, addition of the magnetic dipole term for 1 μm particles does not change α for the superconducting state below the gap [curve (c)] but considerably enhances α in the normal state [curve (d)]. This enhancement is enough to explain the temperature dependence of $(\alpha_s-\alpha_n)$ above the resonance but still to small to explain the normal-state absorption, i.e., the background absorption.

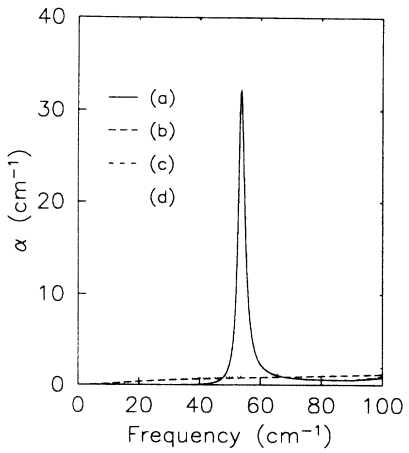

FIG. 19. Effect on the calculated absorptivity of including the magnetic dipole term in the Maxwell-Garnett expression. (a) Superconducting state, electric dipole only, (b) normal state, electric dipole only, (c) superconducting state, electric and magnetic dipole, and (d) normal state with both contributions. It can be seen that including the magnetic term increases the normal-state absorptivity but does not affect the superconducting state absorptivity below the gap.

As shown in Eq. (39), the magnetic dipole absorption is proportional to a^2 in the limit of $a \ll \delta$. However, as the particle size increases, the eddy currents start to be confined near the surface, and the magnetic dipole absorption reaches its maximum near $a=\delta$, after which it starts to decrease. Since the fir skin depth of high-T_c superconducting particles is of the order of 1 μm, the magnetic dipole absorption is near the maximum for the particle sizes studied.

Two extrinsic absorption mechanisms come to mind. During the sample preparation process, especially the grinding process, it is possible that some portion of the samples lose their superconductivity due to chemical instability or strain. We have considered absorption of superconducting particles which are coated by a poorly conducting layer. The low conductivity of the coating enhances the normal-state absorption; however, if the coating is increased enough to make an appreciable contribution to the normal-state α, then the resonance in the superconducting state is damped out. Therefore,the broad background absorption cannot be explained by this extrinsic absorption mechanism.

Since all of the superconductors have a large degree of

atomic disorder, disorder induced absorption[53] in the acoustic phonon spectrum is another possible loss mechanism. Although fir absorption does not occur in the acoustic spectrum of a perfect crystal at $T=0$, the disorder destroys the translational symmetry of the lattice and the acoustic phonon modes become weakly fir active. For example, impurity induced absorption of comparable magnitude[54] is found in KBr:Na^+. Therefore, the anomalously large background absorption we have observed in this study may be related to defect induced phonon absorption that is a direct and unavoidable consequence of the nonstoichiometric materials.

Most infrared[5,6,10] and Raman[55] studies of high-T_c superconductors show that there is absorption below the energy gap that is not in agreement with BCS theory. Even though Thomas *et al.*[12] showed that the reflectivity of $YBa_2Cu_3O_{7-y}$ single crystal approaches 1 below the energy gap, the experimental error is too large to determine the magnitude of the absorption. A more sensitive measurement using direct absorption[56] still shows nonvanishing absorptivity below the gap. The origin of this background absorption is not well known; it is not yet understood whether it comes from material problems or is an intrinsic property. We propose that this absorption below the gap may also stem from disorder-induced phonon absorption[53] and have nothing to do with superconductivity.

E. Possible mechanisms for line broadening

A comparison of Figs. 4 and 16 also shows that there exists a discrepancy between our observed linewidth and the calculated one using a simple phonon-coupling picture. Figure 9(b) also shows that the experimental lines are broader by orders of magnitude than the simple phonon-coupling prediction and that the experimental data do not follow the theoretical linear relationship between the FWHM divided by ω_{sr} and ω_{sr}, given in Eq. (34). There are two kinds of line broadening, homogeneous and inhomogeneous.

Homogeneous broadening could come from an overdamped interband transition or from normal carriers in the superconducting state ("two-fluid model"). The absorption tail of the interband transition can broaden the sphere resonance just like the TO phonon case. However, as mentioned in Sec. V D, the interband transition is located at higher frequency than the phonon, so the effect of the broadening due to the absorption tail of the interband transition should be smaller than that of the phonon. We have tested the two-fluid model and found that the linewidth of the sphere resonance can be explained by assuming that about 50% of the carriers remain normal in the superconducting state. This appears to be an unreasonably large number.

There are three possible inhomogeneous broadening mechanisms: distribution of particle shapes, distribution of T_c among particles due to various sample inhomogeneities, and the dipole-dipole interaction between particles. If the particle is not spherical, the depolarization factor of the particle will change. This change in the depolarization can move the sphere resonance position, so a distribution in the particle shapes will broaden the resonance. We have looked into this possibility and found that we need a very broad distribution of particle shapes (i.e., the aspect ratio of some of the particles should be bigger than 10 or smaller than 0.1) in order to explain the line broadening. From our SEM studies, this kind of broad distribution of particle shapes is not reasonable. There might be distribution of T_c among particles due to sample inhomogeneity. Inhomogeneity of Sr concentration in $La_{2-x}Sr_xCuO_{4-y}$ has been observed by many workers.[57] This distribution of T_c's implies that different particles will have slightly different frequencies, so the resonance could be broadened. The dipole-dipole interaction[58] between particles may or may not lead to broadening of the sphere resonance. Considering the fact that about 20% of our particles are bicrystals, the dipole-dipole interaction between two adjacent particles[59] might be important but a theoretical understanding of the effect on the superconducting particles has not been attempted. Systematic studies are required to understand these details.

F. Comparison with conventional superconductors

Finally, we wish to point out that this sphere resonance is a unique property of the high-T_c materials. In a conventional superconducting metal, the zero crossing of ϵ_1 occurs in the ultraviolet: ϵ_1 is already large and negative in the far infrared, and hence there can be no zero crossing in the region. The high-T_c materials are unique in having a small enough carrier density along the c axis, a sufficiently large scattering frequency and a large positive contribution to ϵ_1 from phonons so that in the normal state $|\epsilon_1-\epsilon_0|<\epsilon_2$ in the far infrared. The condensation of carriers in the superconducting state opens up a relatively large region of small ϵ_2 below the energy gap so that observation of the sphere resonance becomes possible in various oxide superconductors.

VI. SUMMARY

A unique resonance phenomenon has been observed in well-dispersed superconducting oxide particles in Teflon. This feature is explained as novel superconducting sphere resonance within the Maxwell-Garnett approximation, the analytical form of which is derived in this paper. We have shown both theoretically and experimentally that the small-particle geometry is useful since it translates the oscillator strength of the superconducting condensate at zero frequency to finite frequency where it can be probed with spectroscopic methods. Since the oscillator strength of the superconducting condensate is inversely proportional to the square of the London penetration depth, our sphere resonance studies provide a new way to investigate the c-axis London penetration depth. The details of our findings are as follows:

(1) Superconducting sphere resonances have been observed in various Cu oxide superconductors including $La_{2-x}Sr_xCuO_{4-y}$ (where $x<0.2$), $Nd_{1.85}Ce_{0.15}CuO_4$, and $Bi_4Ca_3Sr_3Cu_4O_z$, but not $YBa_2Cu_3O_{7-y}$. Below the lowest phonon frequency, $YBa_2Cu_3O_{7-y}$ particles show

the characteristics of the low-frequency end of the resonance but the complicated phonon spectrum prohibits its clear observation. On the other hand, nonsuperconducting samples including $La_2SrCu_2O_{6+\delta}$ and $La_4BaCu_5O_{13}$ have temperature-independent spectra.

(2) Comparing the measured dc conductivities and resonance positions of $La_{2-x}Sr_xCuO_{4-y}$, $Nd_{1.85}Ce_{0.15}CuO_4$, and $Bi_4Ca_3Sr_3Cu_4O_z$, we find that all the sphere resonances are polarized along the c axis. This assignment shows that the anisotropy ratio of $La_{2-x}Sr_xCuO_{4-y}$ is about 100. The c-axis polarization also agrees with the large magnetic field dependence of the resonance feature.

(3) As the temperature is raised, the resonant peaks shift down in frequency and become weaker, disappearing above T_c. For $La_{1.85}Sr_{0.15}CuO_{4-y}$, the temperature dependence of the peak position follows theoretical predictions using the Mattis-Bardeen theory. However, the temperature dependence of the other samples cannot be described in this way.

(4) The center frequency and strength of the absorption lines increase with Sr doping for the superconducting $La_{2-x}Sr_xCuO_{4-y}$ samples with $x<0.2$. In samples with $x>0.2$, no absorption features are observed up to 180 cm^{-1}, although the samples *are* superconducting. The disappearance of the sphere resonance can be understood by assuming that the expected resonant frequency becomes much larger than 2Δ so that the resonance is overdamped. From this behavior, we can set a lower bound on the c-axis energy gap value of $3.0\ k_BT_c$.

(5) With our sphere resonance which is polarized along the c axis, we can investigate the c-axis London penetration depth, which is difficult to measure by other techniques.[45–49] The observation of the sphere resonance at 53.7 cm^{-1} for $La_{1.85}Sr_{0.15}CuO_{4-y}$ indicates that $\lambda_c(0)=5.8$ μm. The temperature dependence of $\lambda_c(0)/\lambda_c(T)$ for $La_{1.85}Sr_{0.15}CuO_4$ follows the prediction of the empirical "two-fluid" approximation just like the ab-plane London penetration depth measured by other techniques.[45–47]

(6) The experimental sphere resonances show much larger background absorption and much broader linewidth than theoretical predictions based on simple TO phonon coupling. We have suggested several possible mechanisms but more thorough study is required.

ACKNOWLEDGMENTS

We are pleased to acknowledge D. H. Shin for his invaluable help in the TEM measurements. This work was supported by U.S. Defense Advanced Research Projects Agency (DARPA) Grant No. N0014-88-K-0374, by U.S. Army Research Office (ARO) Grant No. DAAL03-86-K-0103 and by National Science Foundation (NSF) Grant No. DMR 87-14600. One of us (S.G.K.) was partially supported by NASA under Grant No. NGT-50264.

[1]R. E. Glover III and M. Tinkham, Phys. Rev. **108**, 243 (1957); D. M. Ginsberg and M. Tinkham, *ibid.* **118**, 990 (1960); P. L. Richards and M. Tinkham, *ibid.* **119**, 575 (1960).

[2]I. Giaever, H. R. Hart, and K. Megerle, Phys. Rev. **126**, 941 (1962); W. L. McMillan and J. M. Rowell, Phys. Rev. Lett. **14**, 108 (1965). An excellent review is given by W. L. McMillan and J. M. Rowell, in *Superconductivity,* edited by R. D. Parks (Marcel Dekker, New York, 1969), Chap. 11.

[3]J. G. Bednorz and K. A. Müller, Z. Phys. B **64**, 189 (1986).

[4]T. K. Worthington, W. J. Gallagher, and T. R. Dinger, Phys. Rev. Lett. **59**, 1160 (1987).

[5]A comprehensive discussion of the optical properties of sintered high-T_c superconductors may be found in a review article by T. Timusk and D. B. Tanner, in *Physical Properties of High Temperature Superconductors,* edited by D. M. Ginsburg (World Scientific, Singapore, 1989).

[6]P. E. Sulewski, T. W. Noh, J. T. McWhirter, and A. J. Sievers, Phys. Rev. B **36**, 5735 (1987); T. W. Noh, P. E. Sulewski, and A. J. Sievers, *ibid.* **36**, 8866 (1987).

[7]M. S. Sherwin, P. L. Richards, and A. Zettl, Phys. Rev. B **37**, 1587 (1988).

[8]F. Gervais *et al.*, Phys. Rev. B **37**, 9364 (1988); M. K. Kelly *et al.*, *ibid.* **38**, 870 (1988); I. Bozovic *et al.*, *ibid.* **38**, 5077 (1988); M. Reedyk *et al.* Phys. Rev. B **38**, 11981 (1988).

[9]S. Tajima, S. Uchida, H. Ishii, H. Takagi, S. Tananka, U. Kawabe, H. Hasegawa, T. Aita, and T. Ishiba, Mod. Phys. Lett. B **1**, 353 (1988).

[10]Z. Schlesinger, R. T. Collins, D. L. Kaiser, and F. Holtzberg, Phys. Rev. Lett. **59**, 1958 (1987).

[11]Z. Schlesinger, R. T. Collins, D. K. Kaiser, F. Holtzberg, G. V. Chandrashekhar, M. W. Shafer, and T. M. Plaskett, Physica C **153-155**, 1734 (1988); R. T. Collins. Z. Schlesinger, G. V. Chandrashekhar, and M. W. Shafter, Phys. Rev. B **39**, 2251 (1989).

[12]G. A. Thomas, J. Orenstein, D. H. Rapkine, M. Capizzi, A. J. Millis, R. N. Bhatt, L. F. Schneemeyer, and J. V. Waszczak, Phys. Rev. Lett. **61**, 1313 (1988).

[13]R. T. Collins, Z. Schlesinger, F. Holtzberg, P. Chaudhari, and C. Feild, Phys. Rev. Lett. **63**, 422 (1989).

[14]T. Timusk, S. L. Herr, K. Kamarás, C. D. Porter, D. B. Tanner, D. A. Bonn, J. D. Garrett, C. V. Stager, J. E. Greedan, and M. Reedyk, Phys. Rev. B **38**, 6683 (1988).

[15]S. W. Tozer, A. W. Kleinsasser, T. Penney, D. Kaiser, and F. Holtzberg, Phys. Rev. Lett. **59**, 1768 (1987).

[16]D. C. Mattis and J. Bardeen, Phys. Rev. **111**, 412 (1958).

[17]R. T. Collins, Z. Schlesinger, R. H. Koch, R. B. Laibowitz, T. S. Plaskett, P. Freitas, W. J. Gallagher, R. L. Sandstrom, and T. R. Dinger, Phys. Rev. Lett. **59**, 704 (1987).

[18]R. A. Laudise, L. F. Schneemeyer, and R. L. Barns, J. Cryst. Growth **85**, 569 (1987); T. Siegrist, L. F. Schneemeyer, J. V. Waszczak, N. P. Singh, R. L. Opila, B. Batlogg, L. W. Rupp, and D. W. Murphy, Phys. Rev. B **36**, 8365 (1987).

[19]T. W. Noh, S. G. Kaplan, and A. J. Sievers, Phys. Rev. Lett. **62**, 599 (1989).

[20]Z. Schlesinger, R. L. Greene, J. Bednorz, and K. A. Müller, Phys. Rev. B **35**, 5334 (1987).

[21]R. Ruppin and R. Englman, Rep. Prog. Phys. **33**, 149 (1970).

[22]L. Genzel and T. P. Martin, Surf. Sci. **34**, 33 (1973).

[23]J. D. Jackson, *Classical Electrodynamics* (Wiley, New York, 1975), Chap. 4.

[24]F. Wooten, *Optical Properties of Solids* (Academic, New York, 1972).

[25]M. Tinkham, *Superconductivity* (Gordon and Breach, New York, 1965), p. 22.

[26]M. Tinkham, *Introduction to Superconductivity* (McGraw-Hill, New York, 1975), Chaps. 1 and 2.

[27]J. C. Maxwell-Garnett, Philos. Trans. R. Soc. London **203**, 307 (1904); **205**, 237 (1906).

[28]J. M. Tarascon, L. H. Greene, W. R. McKinnon, G. W. Hull, and T. H. Geballe, Science **235**, 1374 (1987).

[29]J. B. Torrance, Y. Tokura, A. Nazzal, and S. S. P. Parkin, Phys. Rev. Lett. **60**, 542 (1988).

[30]S. G. Kaplan, T. W. Noh, P. E. Sulewski, H. Xia, A. J. Sievers, J. Wang, and R. Raj, Phys. Rev. B **38**, 5006 (1988).

[31]Y. Tokura, H. Takagi, and S. Uchida, Nature **337**, 345 (1989).

[32]A number of articles and reference on inhomogeneous media may be found in *Electrical Transport and Optical Properties of Inhomogeneous Media (Ohio State University, 1977)*, Proceedings of the First Conference on the Electrical Transport and Optical Properties of Inhomogeneous Media, AIP Conf. Proc. No. 40, edited by J. C. Garland and D. B. Tanner (AIP, New York, 1978).

[33]C. F. Bohren and D. R. Huffman, *Absorption and Scattering of Light by Small Particles* (Wiley, New York, 1983), Chap. 8.

[34]E. A. Lynton, *Superconductivity* (Methuen, London, 1964), Chap. 10.

[35]We tested this argument with a numerical calculation. The oscillator strength of the c-axis resonance was estimated using the curve shown in Fig. 15(c) and integrating over the region where α_s is large than α_n. This area is equal to 110 cm^{-2}, reasonably close to 142 cm^{-2}, the value obtained from multiplying Eq. (31a) by $\frac{1}{3}$, which is the contribution to the c axis in the anisotropic Maxwell Garnett Theory (MGT), as discussed in Sec. III B 3.

[36]L. D. Landau and E. M. Lifshitz, *Electrodynamics of Continuous Media* (Pergamon, Oxford, 1960), Chap. 45.

[37]N. E. Russell, J. C. Garland, and D. B. Tanner, Phys. Rev. B **23**, 632 (1981); S.-I. Lee, T. W. Noh, and J. R. Gaines, *ibid.* **32**, 3580 (1985).

[38]J. M. Bassat, P. Odier, and F. Gervais, Phys. Rev. B **35**, 7126 (1987).

[39]Y. Hidaka, Y. Enomoto, M. Suzuki, M. Oda, and T. Murakami, Jpn. J. Appl. Phys. **26**, L377 (1987); S. Shamoto, M. Onoda, M. Sato, and S. Hosoya, Solid State Commun. **62**, 479 (1987); M. Sato, Physica C **153-155**, 38 (1988).

[40]S. Martin, A. T. Fiory, R. M. Fleming, L. F. Schneemeyer, and J. V. Waszczak, Phys. Rev. Lett. **60**, 5102 (1988); S. Martin, A. T. Fiory, R. M. Fleming, G. P. Espinosa, and A. S. Cooper, Appl. Phys. Lett. **54**, 72 (1989).

[41]P. E. Sulewski, Ph.D. thesis, Cornell University, 1988 (unpublished), p. 159.

[42]G. L. Carr and D. B. Tanner, Phys. Rev. Lett. **62**, 2763 (1989).

[43]T. W. Noh, S. G. Kaplan, and A. J. Sievers, Phys. Rev. Lett. **62**, 2764 (1989).

[44]Z. Zou and T. C. Hsu, Mod. Phys. Lett. B **2**, 939 (1988).

[45]L. Krusin-Elbaum, R. L. Greene, F. Holtzberg, A. P. Malozemoff, and Y. Yeshurun, Phys. Rev. Lett. **62**, 217 (1989).

[46]Y. J. Uemura, V. J. Emery, A. R. Moodenbaugh, M. Suenaga, D. C. Johnston, A. J. Jacobson, J. T. Lewandowski, J. H. Brewer, R. F. Kiefl, S. R. Kreitzman, G. M. Luke, T. Riseman, C. E. Stronach, W. J. Kossler, J. R. Kempton, X. H. Yu, D. Opie, and H. E. Schone, Phys. Rev. B **38**, 909 (1988).

[47]D. R. Harshman, L. F. Schneemeyer, J. V. Waszczak, G. Aeppli, R. J. Cava, B. Batlogg, L. W. Rupp, E. J. Ansaldo, and D. Ll. Williams, Phys. Rev. B **39**, 851 (1989).

[48]R. Felici, J. Penfold, R. C. Ward, E. Olsi, and C. Matacotta, Nature **329**, 523 (1987).

[49]A. T. Fiory, A. F. Hebard, P. M. Mankiewich, and R. E. Howard, Phys. Rev. Lett. **61**, 1419 (1988).

[50]For a survey of the early literature, see T. Forgan, Nature **329**, 483 (1987).

[51]S. E. Inderhees, M. B. Salamon, N. Goldenfeld, J. P. Rice, B. G. Pazol, D. M. Ginsberg, J. Z. Liu, and G. W. Crabtree, Phys. Rev. Lett. **60**, 1178 (1988).

[52]R. P. Devaty and A. J. Sievers, Phys. Rev. Lett. **52**, 1344 (1984); and (unpublished).

[53]A. S. Barker and A. J. Sievers, Rev. Mod. Phys. **47**, S1 (1975).

[54]R. W. Ward and T. Timusk, Phys. Rev. B **5**, 2351 (1972).

[55]S. L. Cooper, M. V. Klein, B. G. Pazol, J. P. Price, and D. M. Ginsberg, Phys. Rev. B **37**, 5920 (1988).

[56]D. Miller, T. W. Kenney, P. L. Richards, Bull. Am. Phys. Soc. **34**, 792 (1989).

[57]See, for example, P. E. Sulewski, A. J. Sievers, S. E. Russek, H. D. Hallen, D. K. Lathrop, and R. A. Buhrman, Phys. Rev. B **35**, 5330 (1987).

[58]Z. Schlesinger, L. H. Greene, and A. J. Sievers, Phys. Rev. B **32**, 2721 (1985).

[59]R. G. Barrera, G. Monsivais, and W. L. Mochán, Phys. Rev. B **38**, 5371 (1988).

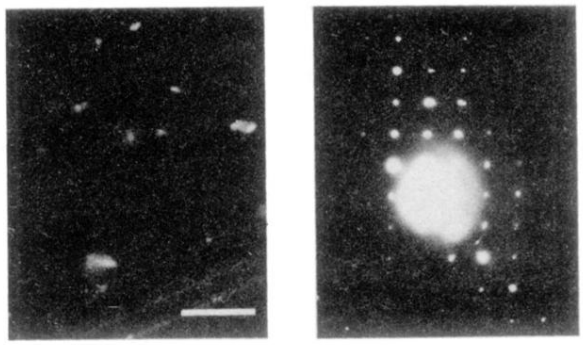

FIG. 3. (a) An SEM picture of 1 mol % $La_{1.8}Sr_{0.2}CuO_{4-y}$ particles in Teflon. The solid bar in the figure indicates 10 μm. The photograph shows that the particles are well separated. (b) The electron diffraction pattern of a typical $La_{1.8}Sr_{0.2}CuO_{4-y}$ particle in the Teflon matrix. This TEM picture shows that the particle is composed of one single crystal. The diffuse scattering is from the Teflon. About 80% of the particles are single crystals, and the remainder are bicrystals.